UNIVERSIDADE D
COIMBRA

Francisco Alexandre Pereira Jesus

# EFFECT OF CHRISTMAS TREE LOADING PATTERN ON FATIGUE CRACK GROWTH

**Dissertação no âmbito do Mestrado Integrado em Engenharia Mecânica, na especialidade de Produção e Projeto orientada pelo Professor Doutor Diogo Mariano Simões Neto e pelo Mestre Edmundo Rafael de Andrade Sérgio e apresentada ao Departamento de Engenharia Mecânica da Faculdade de Ciências e Tecnologia da Universidade de Coimbra**

Julho de 2022

1 2 9 0

FACULDADE DE CIÊNCIAS E TECNOLOGIA
UNIVERSIDADE D COIMBRA

# Effect of Christmas Tree Loading Pattern on Fatigue Crack Growth

Submitted in Partial Fulfilment of the Requirements for the Degree of Master's in Mechanical Engineering in the speciality of Production and Project

# Efeito do Padrão de Carga em Forma de Árvore de Natal na Propagação de Fendas por Fadiga


**Author**

**Francisco Alexandre Pereira Jesus**

**Advisors**

**Professor Doutor Diogo Mariano Simões Neto**

**Mestre Edmundo Rafael de Andrade Sérgio**


**Committee**

| | |
|---|---|
| **Chair** | **Professor Doutor José Domingos Moreira da Costa**<br>**Professor Associado com Agregação da Universidade de Coimbra** |
| **Member** | **Professor Doutor Ricardo Nuno Madeira Soares Branco**<br>**Professor Auxiliar da Universidade de Coimbra** |
| **Advisor** | **Mestre Edmundo Rafael de Andrade Sérgio**<br>**Mestre da Universidade de Coimbra** |

**Coimbra, July, 2022**

To my mother and my nephews.

*It's not what happens to you that*
*determines how far you will go in life;*
*it is how you handle what happens to you.*
Zig Ziglar

# ACKNOWLEDGEMENTS

First, I would like to express my deep gratitude to my advisor, Professor Diogo Neto for his availability, patience, guidance, and knowledge transmitted throughout this semester.

To Professor Fernando Antunes for his support and concern he always had with me along this path.

To my co-advisor and friend Edmundo Sérgio for his help not only during this semester but also throughout my academic career.

To Professor Marta Oliveira for the availability of the model and for programming the non-contact simulations in DD3IMP.

To the Technology Group of the Mechanical Engineering Department for the availability of the finite element program DD3IMP.

To my friends for all the support and for all the moments lived in this city, which will never be forgotten.

To my nephews for your affection and unconditional support, which gave me the strength to make this dream come true.

To the rest of my family who never let me give up no matter how hard it was.

Finally, a special thanks to my mother for her support, effort, and dedication during this stage of my life, because she is the person to whom I owe everything I am and have accomplished so far.

This research work was sponsored by national funds from the Portuguese Foundation for Science and Technology (FCT) under the project with reference PTDC/EME-EME/31657/2017 and by European Regional Development Fund (ERDF) through the Portugal 2020 program (PT2020) and the Centro 2020 Regional Operational Programme (CENTRO-01-0145-FEDER-031657).

# Abstract

Most mechanical components are subject to cyclic or dynamic loads, which can cause failure in service. The main failure mode of such equipment is the fatigue phenomenon. Thus, fatigue design is crucial to predict the service life of components and avoid catastrophic consequences, especially in economic terms and in the loss of human lives. The prediction of service life is usually done by assessing fatigue crack growth (FCG), using $da/dN - \Delta K$ curves. However, this methodology presents some limitations as the stress intensity factor, $K$, is an elastic parameter and the phenomena occurring at the crack tip are irreversible. These limitations led to the study of nonlinear parameters, which allow a better understanding of the FCG, such as the plastic crack tip opening displacement (CTOD) used in this work.

This study aims to evaluate the effect of variable amplitude loadings on fatigue crack growth, in compact-tension (CT) specimens produced with an AA2024-T351 aluminium alloy. Specifically, it is intended to obtain the prediction of the crack propagation rate, when the specimen is subjected to a complex loading pattern, named “Christmas Tree Spectrum”. The numerical study was conducted using the in-house developed finite element code DD3IMP. The crack propagation is controlled by the plastic deformation value at the crack tip.

Results present a good agreement between FCG and CTOD curves and are similar for both simulations subjected to constant amplitude and variable amplitude loading, except for the High Frequency pattern. The plastic deformation tends toward the same value regardless of the simulation under study, when considering the same time interval. Furthermore, both the propagation rate and plastic deformation tend towards higher values in the non-contact simulations, thus concluding that the crack closure phenomenon is relevant in this context.

**Keywords:** Fatigue Crack Growth, Variable Amplitude Loading, CTOD, Plastic Strain, Crack Closure, Numerical Simulation.

# Resumo

A maioria dos componentes mecânicos está sujeito a cargas cíclicas ou dinâmicas, que podem provocar falhas em serviço. O principal modo de ruína destes equipamentos é o fenómeno de falha de fadiga. Deste modo, é importante o dimensionamento à fadiga para prever a vida útil dos componentes e evitar consequências catastróficas, especialmente económicas e humanas. A previsão da vida útil é obtida é habitualmente estudada através da propagação de fendas por fadiga (PFF), utilizando curvas $da/dN - \Delta K$. Uma vez que o fator de intensidade de tensão, $\Delta K$, é um parâmetro elástico e os fenómenos que ocorrem na extremidade da fenda são irreversíveis, esta metodologia apresenta algumas limitações. Assim, essas limitações levam à procura de parâmetros não lineares para uma melhor compreensão da PFF, como por exemplo o CTOD plástico, como é utilizado neste trabalho.

Esta dissertação tem como objetivo principal o estudo do efeito de carregamentos de amplitude variável na propagação de fendas de fadiga em provetes de tensão compacta (CT) de uma liga AA2024-T351. Assim, pretende-se obter a previsão da velocidade de propagação da fenda, quando o provete está sujeito a um carregamento complexo denominado "*Christmas Tree Spectrum*". Este estudo realizou-se numericamente recorrendo ao programa de elementos finitos DD3IMP, assumindo que a propagação da fenda é controlada pelo valor da deformação plástica na extremidade da fenda.

Verificou-se que a PFF e as curvas de CTOD são semelhantes tanto para as simulações submetidas a um carregamento de amplitude constante como para as de amplitude variável, com exceção do padrão High Frequency. A deformação plástica tende para o mesmo valor independentemente da simulação em estudo, desde que seja durante o mesmo intervalo de tempo. Além disso, tanto a velocidade de propagação como a deformação plástica tendem para valores superiores nas simulações sem contacto, concluindo assim que o fenómeno de fecho de fenda é relevante neste contexto.

**Palavras-chave:** Propagação de Fendas por Fadiga, Carga de Amplitude Variável, CTOD, Deformação Plástica, Fecho de Fenda, Simulação Numérica.

# Contents

# LIST OF FIGURES

# LIST OF TABLES

# LIST OF SIMBOLS AND ACRONYMS/ABBREVIATONS

## List of Symbols

$a$ – Crack length

$a_0$ – Initial crack length

$C, m$ – Constants of the Paris-Erdogan law

$C_X$ – Parameter of the Armstrong & Frederick kinematic law

$da/dN$ – Fatigue crack growth rate, measured in length/cycle

$da/dt$ – Fatigue crack growth rate, measured in length/second

$\mathcal{F}$ – Function defining the yielding condition

$F$ – Applied load

$F_{\max}$ – Maximum load in a loading cycle

$F_{\min}$ – Minimum load in a loading cycle

$F_{\text{open}}$ – Crack opening load

$F_{\text{closure}}$ – Crack closing load

$K$ – Stress intensity factor

$K_{1C}$ – Fracture toughness

$K_{\max}$ – Maximum stress intensity factor

$K_{\min}$ – Minimum stress intensity factor

$K_{\text{open}}$ – $K$ value corresponding to crack opening

$R$ – Stress ratio

$X$ – Deviatoric back-stress tensor

$X_{\text{sat}}$ – Deviatoric back-stress tensor parameter

$Y$ – Geometric parameter

$\delta_{\text{e}}$ – Elastic CTOD range

$\delta_{\text{p}}$ – Plastic CTOD range

$\Delta K$ – Stress intensity factor range

$\Delta K_{\text{eff}}$ – Effective stress intensity factor range

$\Delta K_{\text{th}}$ – Fatigue threshold

$\bar{\varepsilon}^p$ – Equivalent plastic strain

$\bar{\varepsilon}_c^p$ – Critical plastic deformation value

$\sigma'$ – Deviatoric Cauchy stress tensor

$\bar{\sigma}$ – Equivalent stress

$\sigma$ – Nominal stress

$\sigma_{max}$ – Maximum stress

$\sigma_{min}$ – Minimum stress

$\sigma_Z$ – Normal stress componente

$\nu$ – Poisson´s ratio

## Acronyms/Abbreviations

AA – Aluminium Alloy

CJP – Christopher James Patterson (model)

COD – Crack Opening Displacement

CT – Compact-Tension

CTOD – Crack Tip Opening Displacement

DD3IMP – Deep Drawing 3D IMPlicit finite element solver

FCG – Fatigue Crack Growth

LEFM – Linear Elastic Fracture Mechanics

OICC – Oxidation Induced Crack Closure

PDMR – Path-Dependent Maximum Range

PICC – Plasticity Induced Crack Closure

RICC – Roughness Induced Crack Closure

TPS – Total Plastic Strain

SSY – Small Scale Yielding

# 1. INTRODUCTION

## 1.1. Motivation

The human being is distinguished by his logical and rational ability to create and improve inventions given his craving for efficiency and convenience, being necessary to perform several steps in the development of a project. This whole process begins by gathering all the knowledge about the subject under study, from projects already developed to date and/or information and concepts, to improve it.

Most mechanical components are subjected to loads that vary over time. These components can fail in service due to various factors and phenomena with fatigue being particularly prevalent. Indeed, around 80% to 90% of the ruin of parts and structures, operating in the room temperature zone and subjected to cyclic or dynamic loadings are related to fatigue failure [1]. Fatigue is a slow and irreversible process of plastic deformation that depends on the number of cycles that a given material is subjected to. Moreover, this process depends on several factors, such as component geometry, material properties, loading type and orientation, environmental conditions, among others, thus making it extremely complex. Furthermore, fatigue damage is caused by stress levels below the tensile strength limit or even below the yield strength limit [2]. Finally, this process consists of three distinct phases, crack initiation, crack propagation and finally final fracture. The total fatigue life is equal to the sum of the lives of the initiation and propagation phases. In many situations, namely in the presence of defects or stress concentrators, the propagation time is dominant.

Predicting unstable fracture or propagation of a pre-existing crack is the most fundamental issue in fracture mechanics [3]. As industrial components are constantly subjected to cyclic loadings, failure can bring catastrophic consequences both at the human, economic and environmental level. Thus, it is necessary to perform tests that help us understand and predict the behaviour of materials under these conditions. One of the methods to evaluate fatigue performance is through experimental results focused on material properties. However, since it is not possible to change material properties individually, as they are interdependent, improving fatigue resistance becomes an extremely difficult, time

consuming and expensive process. Alternatively, the fatigue behaviour can be evaluated numerically. Through this method it is possible to obtain a very close representation of the physical behaviour, allowing a better understanding of the effect of parameters on fatigue process. This methodology is very interesting to isolate the effect of the variables affecting the fatigue process, and therefore to develop parametric studies.

Fatigue crack growth (FCG) has been studied for decades; however, several aspects are still controversial [4]. Most studies are based on constant amplitude loading conditions, since it is extremely difficult to perform studies on variable amplitude loads due to the random nature and consequently vastness of patterns. The lifetime of the components is obtained through the crack propagation rate $da/dN$ and the range of the intensity factor $\Delta K$, resulting in the well known $da/dN - \Delta K$ curves [5]. This methodology has some inconsistencies and limitations. In fact, $\Delta K$ is an elastic parameter, and fatigue crack propagation is related to nonlinear and irreversible mechanisms that occur at the crack tip zone. To overcome this drawback, other methodologies have been proposed, such as the crack closure concept, T-stress, CJP model, J-integral, and CTOD, among others. The research team proposed the use of plastic CTOD and more recently the cumulative plastic strain to predict FCG rate. This last approach was used to study the effect of overloads, load blocks and the Superblock 2020 load pattern, which is composed of constant amplitude load blocks separated by overloads. However, it is important to study more elaborate load patterns, which approximate the patterns actually applied to real components, such as automobiles and airplanes.

## 1.2. Objectives

This dissertation aims to study the effect of variable amplitude loading conditions on FCG. For this purpose, an aluminium alloy, AA2024-T351, CT specimen is subjected to a variable amplitude loading pattern called "Christmas Tree Loading". The fatigue crack propagation is predicted numerically using the in-house developed finite element code DD3IMP (Three-Dimensional Elasto-Plastic Finite Element Program) [6], [7]. The crack propagation is here controlled by the cumulative plastic deformation at the crack tip. Additionally, two different constant amplitude loading spectrums are applied to the same specimen geometry in order to assess the effect of the variable amplitude loading on fatigue crack growth.

## 1.3. Layout of The Thesis

This dissertation is divided into five chapters, where the numbering and main objective of each are presented below:

- **Chapter 1 – Introduction:** Introduction to the subject under study, as well as its objectives and report structure.
- **Chapter 2 – Literature Review:** Descriptions of the most important concepts and definitions necessary for the interpretation of the results. Additionally, the advantages and limitations of the methodology used to carry out this thesis are presented.
- **Chapter 3 – Numerical Model:** Presentation and description of the numerical model used in the numerical simulations. The input files to the code are described, as well as the mesh of the specimen and boundary conditions. The propagation criterion, based on plastic deformation is also presented.
- **Chapter 4 – Numerical Results and Discussion:** Presentation and discussion of the results obtained for the different evaluated loading patterns. The obtained correlations and the fatigue crack growth rates are discussed.
- **Chapter 5 – Conclusions:** Presentation of the main conclusions obtained in this study. In addition, some proposals are suggested for future work.

# 2. FATIGUE CRACK GROWTH

## 2.1. Fatigue Phenomenon

In 1829, the first discoveries about material fatigue were made by Wilhelm August Julius Albert [8]. Since then, the study of this type of failure has become increasingly important, aiming to understand the processes of crack initiation and propagation. In fact, fatigue can be defined as the "process of progressive and localized plastic deformation, occurring in a material subjected to cyclic stresses and strains, at high stress concentration locations that may culminate in cracks or complete fracture after a sufficient number of fluctuations." [9].

As mentioned earlier, fatigue is composed by three phases, assuming no initial cracks in the component.

- **Crack initiation –** The first phase develops typically on the surface of the part, at point(s) where the stresses concentration is higher. Generally, this phase occurs due to the presence of some defect or due to the effect of roughness, concentrating plastic deformation by the action of repeated and continuous application of loads. This phase is divided into two stages, nucleation and microscopic crack growth. Nucleation is identified by the formation of slip lines on the surface, representing crack initiation. Microscopic crack growth can occur by ductile or brittle striation, coalescence of microcavities, or microcleavage. Due to the presence of microstructural barriers, it is characterized by slow crack growth rates.
- **Crack propagation –** This phase is characterized by the progressive increase of the crack propagation speed, usually in the direction perpendicular to the load application. The crack paths are often not linear, showing Zigzag patterns, resulting from material microstructure, or even deflection, due to complex loadings.
- **Final fracture –** The last phase occurs when the crack length reaches a critical value. The crack propagates at a very high and extremely unstable rate,

originating the fracture of the material when the resistant area is no longer able to support the applied loads.

Several studies have been conducted to understand the effects of loading parameters, for example Paris and Erdogan [10], Erdogan and Ratwani [11] and, Hartman and Schijve [12]. A mechanical structure generally experiences variable amplitude loads, however most of the studies conducted so far have been on constant amplitude and variable amplitude with low complexity. This is because variable amplitude loads make the fatigue process even more complex, and because there is a vastness of load patterns. Usually only overloads, underloads and load blocks are studied, which does not replicate the real load patterns.

## 2.2. Concepts of Linear Elastic Fracture Mechanics (LEFM)

As mentioned before, FCG is related to nonlinear and irreversible mechanisms that occur at the crack tip. However, the stress distribution around the crack tip is usually studied using LEFM. This theory was proposed by Irwin [13], in 1958, to describe the behaviour of brittle fracture. Later, it was adapted for FCG problems.

Despite the importance of LEFM it can only be applied to cases where the nonlinear behaviour is so small that it can be neglected. This means that the validity of this theory requires the region of nonlinear behaviour to be very small relatively to the crack length and other dimensions of the part in study (Small Scale Yielding, SSY, condition). In fact, the intensity and distribution of the stress at the crack tip results in the formation of a plastically deformed zone. Additionally, the stress intensity at the crack tip depends on numerous factors, such as the nominal stress applied to the part, the size, shape, and orientation of the crack. Since LEFM does not account for plastic deformation, the damage at the crack tip is assumed to be controlled by the elastic field [14].

The fundamental principle of LEFM is the characterization of the stress field surrounding the crack tip. This is usually achieved through the stress intensity factor, $K$, which is the main parameter responsible for the elastic stress and strain field in the regions near the crack tip. The stress intensity factor can be obtained by:

$$K = Y\sigma\sqrt{\pi a}, \tag{2.1}$$

where, $Y$ is a dimensionless parameter that depends on the landing state and part and crack geometries, $\sigma$ is the nominal applied stress and $a$ is the crack length.

## 2.3. ΔK – Based Fatigue Crack Growth Analysis

The service life of a component is usually accessed through the FCG rates, using the $da/dN - \Delta K$ curves. Since the value of the stress intensity factor varies over time when the component is subjected to cyclic loading, it is replaced by its range, $\Delta K$, given by:

$$\Delta K = K_{\max} - K_{\min}, \tag{2.2}$$

where $K_{\max}$ and $K_{\min}$ consist in the stress intensity factors at maximum and minimum loads, respectively.

To represent the $da/dN - \Delta K$ curves, it is necessary to know several parameters, such as $\Delta K$, $a$, and the maximum and minimum stresses, $\sigma_{\max}$ and $\sigma_{\min}$, respectively, among others. Additionally, it is possible to identify three different regions in these curves, as shown in Figure 2.1.

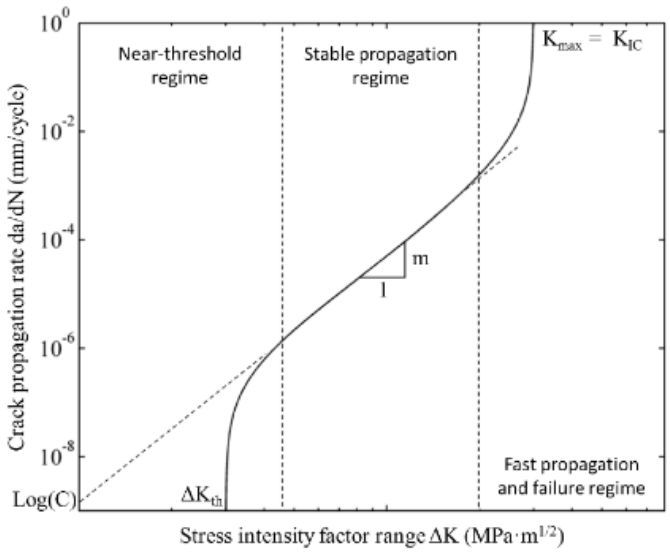


**Figure 2.1 – $da/dN$ versus ΔK curve on log-log scale, adapted from [15].**

- **Near-threshold regime** – This regime is characterized by a sharp increase in the propagation rate with increasing values of $\Delta K$. In addition, there is no crack propagation for values below the fatigue threshold, $\Delta K_{\text{th}}$, which, therefore, plays an important role for safety design regarding fatigue damage tolerance approach. The value of $\Delta K_{\text{th}}$ decreases by increasing the mean stress, and is affected by crack geometry and size, component dimensions, material properties, loading parameters and surrounding environment. This parameter can be obtained experimentally.

- **Stable propagation regime** – In this regime, also known as the Paris-Erdogan regime, the $da/dN - \Delta K$ curve evolves linearly on a bi-logarithmic scale. In this region, the curve is governed by the Paris-Erdogan equation [10]:

$$\frac{da}{dN} = C(\Delta K)^m, \tag{2.3}$$

  in which $C$ and $m$ are parameters that depend on the material, the environmental conditions, and the stress ratio, $R$, given by:

$$R = \frac{\sigma_{\min}}{\sigma_{\max}}. \tag{2.4}$$

- **Final failure regime** – In the upper regime, there is a sharp rise in the propagation rate with the increase of $\Delta K$, as the value of $K_{\max}$ approaches $K_{1C}$. In fact, when $K_{\max}$value equals the $K_{1C}$ value, material fracture occurs.

## 2.4. Issues Regarding LEFM

The methodology used with the LEFM theory presents several advantages, such as the fact that $K$ values may be obtained analytically, where several solutions currently exist for different crack geometries [16]. In particular, for long cracks, LEFM presents good results where the linearity evidenced by Paris law is greatly contemplated. Despite all these advantages, several problems have been identified in this methodology, such as:

- Inability to predict the influence of the stress ratio ($R$) [17];
- Inability to predict the influence of loading history;
- Abnormal behaviour observed in small cracks;
- Dimensional problems of the $da/dN - \Delta K$ curve;
- $da/dN$ curves are obtained for constant amplitude loadings, which is an important limitation since real life loadings usually present varying amplitudes and stress ratios;
- LEFM theory is valid only in the prevalence of the SSY condition. As mentioned before, this condition is true, when the plastic zone is restricted to a sufficiently small extension in relation to the dimensions of the crack or structure.

## 2.5. Complementary Concepts

Since the LEFM-based theory has several limitations regarding the fatigue crack propagation process, different theories and parameters have emerged, trying to describe this phenomenon with a higher level of accuracy.

One of the best-known approaches is the crack closure phenomenon which was firstly addressed by Elber [18]. He observed that a fatigue crack could be closed even while subjected to tensile loads. Consequentially, stresses lower than the crack opening stress are not expected to cause crack propagation. This phenomenon occurs when the crack faces contact each other, inducing a protective effect on the crack tip. Therefore, crack closure improves fatigue resistance [19], since it is assumed that only the range of the load cycle during which the crack is open contributes to crack propagation.

Crack closure can be caused by several mechanisms, such as the (i) Plasticity Induced (PICC) [20]; (ii) Oxide Induced (OICC) [21] and (iii) Roughness Induced (RICC) [22] mechanisms, as presented in Figure 2.2, respectively.

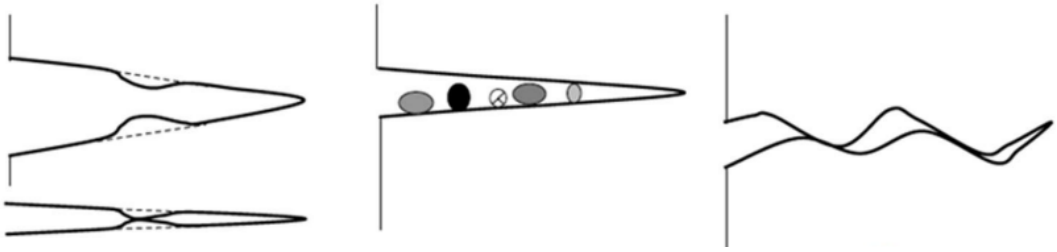

(i) (ii) (iii)

**Figure 2.2 – Schematic representation of the main crack closure mechanisms, adapted from [23].**

Fatigue crack propagation laws that include the effect of fatigue crack closure are based on the relationship between fatigue crack growth rate ($da/dN$) and the effective range of the stress intensity factor, $\Delta K_{\text{eff}}$ [24]. The general FCG formula for the stable propagation regime, which takes into account the effect of crack closure, takes the following form:

$$\frac{da}{dN} = C(\Delta K_{\text{eff}})^m. \tag{2.5}$$

The effective stress intensity factor range, $\Delta K_{\text{eff}}$, is then given by:

$$\Delta K_{\text{eff}} = K_{\max} - K_{\text{open}}, \tag{2.6}$$

where $K_{\text{open}}$ is the stress intensity factor below which the crack remains closed. Figure 2.3 depicts the range of effective stress intensity factors and the relevant stress intensity factors.

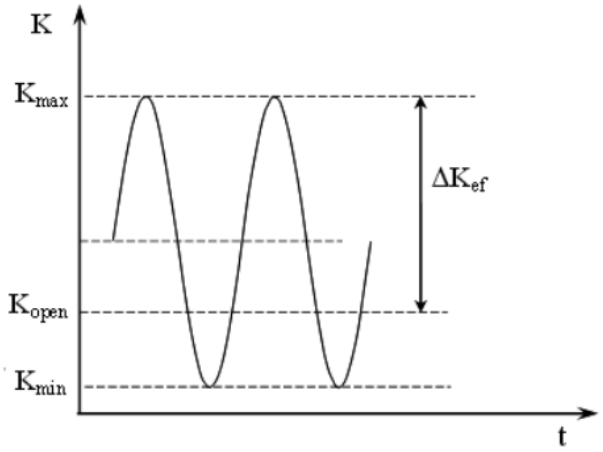


**Figure 2.3 – Schematic representation of the effective stress intensity factor. Adapted from [18].**

Despite not being consensual in scientific circles devoted to FCG analysis, the crack closure concept provided a better understanding of the effect of variable parameters, such as loading history and microstructure. In addition to crack closure other relevant approaches have emerged, such as the concept of partial crack closure [25], [26], T-stress [27], [28] and the CJP model [29].

Partial crack closure proposes that the loading spectrum below the crack opening load contributes to fatigue damage since, according to the authors [25], [26], the existing contact between the crack flanks does not occur immediately behind the crack tip. Another important concept is the T-stress where it is necessary to measure the stress parallel to the crack flanks. This approach was used to quantify the size and shape of the plastic zone at the crack tip by varying the sign and magnitude of T-stress. Finally, the Christopher James Patterson (CJP) model describes the stress field around the crack tip using various modified stress intensity factors.

As mentioned before, the stress intensity factor is an elastic parameter and all the methodologies stated above are based on this parameter. Thus, nonlinear parameters were proposed to replace $\Delta K$ in order to have a better understanding of what happens at the crack tip.

## 2.6. Elasto-Plastic Fracture Mechanics

When a component is subjected to cyclic loading, three distinct zones are developed at the crack tip. Figure 2.4 shows the representation of these zones in tensile loading mode.

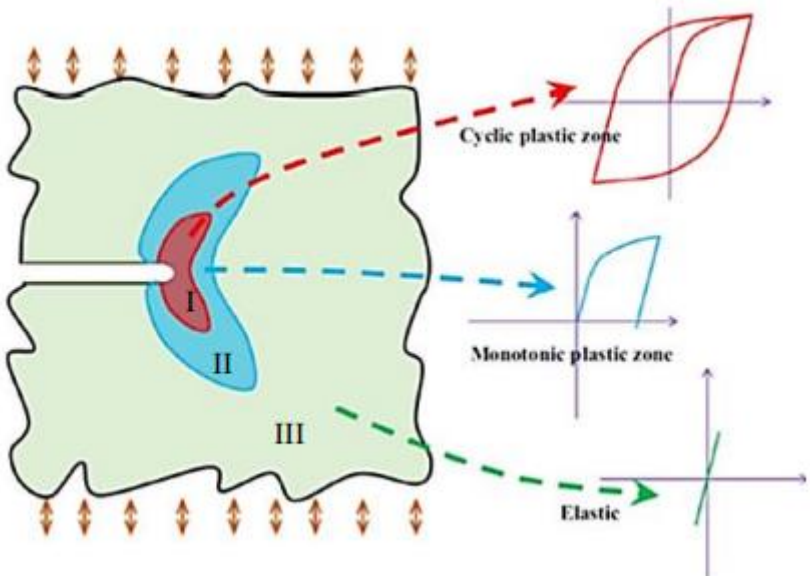


**Figure 2.4 – Induced zones, around the crack tip, and their responses in stress-strain curves, adapted from [30].**

Each zone can be characterized as follows:

- **Zone I – Cyclic Plastic Zone:** This zone stands out for the hysteresis cycle, in stress-strain plots, being affected by $R$ and loading range.
- **Zone II – Monotonic Plastic Zone:** A plastic deformation point is reached in this zone during loading. When the material is unloaded an elastic-type unloading occurs.
- **Zone III:** This is the zone farthest from the crack tip, where the material has an elastic behaviour.

It is important to note that the size of the plastic zone at the crack tip varies depending on the stress state developed at the yielding point and is also influenced by the yield stress of the material itself. Furthermore, the size of the plastic zone is larger under plane stress conditions than under plane strain conditions. This occurs because under plane stress conditions, the normal stress component, $\sigma_Z$, is zero but out of plane deformations, $\varepsilon_z$, are allowed. However, under plane strain conditions, the stress component takes non-zero values, restricting plastic flow.

### 2.6.1. Crack Tip Opening Displacement – CTOD

In 1961, Wells [31] proposed a measure of fracture toughness by noticing that the crack faces separated before fracture for materials that had a high degree of plasticity. This

way, the Crack Tip Open Displacement, CTOD, emerged as a parameter for measuring the displacement of the crack flanks. While CTOD is used for measurements near the crack tip, COD (Crack Opening Displacement) is used for measurements farther from the crack tip.

The CTOD parameter is of particular importance when characterizing the fracture behaviour, and two definitions have been developed. The first one, proposed by Wells [31] focuses on the displacement normal to the crack plane relative to the original position of the crack tip, i.e., it measures the opening displacement of the original crack tip. The other definition was developed by Rice [32] and measures the displacement at an intersection of a 90° vertex with the slits of the slit. These two definitions of the CTOD concept are shown in Figure 2.5.

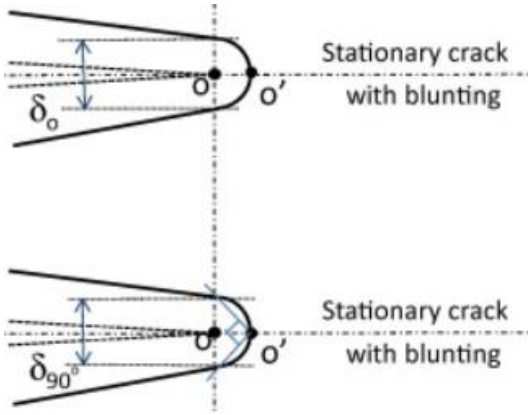


**Figure 2.5 – Definitions of CTOD. Adapted from [33].**

Over the years, several authors proposed FCG relations using the CTOD concept. More recently, Antunes *et al* [5], [34], [35], propose the use of the plastic CTOD, $\delta_{\mathrm{p}}$, at the crack tip instead of the parameter $\Delta K$. Through this parameter substitution, the model is now defined by $da/dN - \delta_{\mathrm{p}}$, with the advantage of integrating the crack closure phenomenon in a natural way. Furthermore, Antunes discloses in his works the hypothesis of quantifying the plastic deformation level through $\delta_{\mathrm{p}}$, assuming that the FCG is directly linked to plastic strain.

Predicting FCG through CTOD requires accurate measurements at the crack tip zone. In fact, an underestimation of FCG rate would consequently result in unstable propagation and ultimately failure. On the other hand, an overestimation must also not occur as this can lead to defects of very small size and consequently increase the inspection intervals. Numerically, the measurement of the CTOD is usually obtained at the node just before the crack tip.

## 2.7. Models for Variable Amplitude Loads

Over the years, several models for predicting FCG under variable amplitude loading have been proposed, addressing several aspects of variable amplitude fatigue. The reference list includes more than 290 publications [36].

The model proposed by Wheeler [37], is based on the analysis of the size of the plastic zone ahead of the crack tip. This was one of the first models to emerge and has proven successful for estimating fatigue crack growth life under constant amplitude loading spectra interrupted by single or repeated overloads. However, it presents some limitations when dealing with underload cycles that occur periodically within a load spectrum [38].

The model proposed by Noroozi *et al*. [39] is based on the elastic-plastic strain-stress behaviour that characterizes the material response in the crack tip region. According to Skorupa [40], this model is grouped to the so-called "Residual stress-based models". This model was later modified to be applicable for all types of variable amplitude loading spectra [41]. The “residual stress-based models” are widely used and are based on calculations of the yield zone size ahead of the crack tip. There is another category of models based on the crack closure approach, which considers plastic deformation and the interaction of the crack tip with the plastic wake [42]. Later, models proposed by Elber [43] were used to simulate crack growth rates under varying amplitude loads. More recent proposals are based on combinations of Wheeler's and Newman's crack closure model based on the strain energy density factor [42].

There is still no universal model to study the FCG process due to the large number and complexity of mechanisms associated with the phenomenon. Skorupa [36] studied load interaction phenomena using several sequences of simple variable amplitude loadings, of which we highlight two-level blocks (High-Low, Low-High and step in both maximum and minimum load). However, sequences with overloads, single overloads, overload blocks, periodic overload blocks and combinations of overloads and underloads were also addressed. Recently, Silva [44] also conducted studies on the behaviour of simple variable amplitude loads with two-level blocks (High-Low, Low-High, Underload).

In 1968, Matsuishi and Endo [45], [46] introduced the first accepted method used to extract closed-load cycles, the Rainflow Cycle. This analogy is derived from the similarity of this method to the rain flow, running off the edges of a roof. This method specifically identifies hysteresis cycles within a time history of load, stress, or strain [47]. Currently,

there are several different algorithms for the Rainflow Cycle counting method, such as the three-point [48], [49] and four-point cycle counting techniques [50].

The three-point cycle counting method continuously evaluates the load history when a peak or valley occurs. The basic rule for counting the points is illustrated in Figure 2.6. If the load history is periodic, it needs to be readjusted by starting the count with the peak or valley with the largest absolute magnitude. Subsequently, the cycle identification rule is applied to check three consecutive points from the first cycle, until a closed cycle is defined [47]. This procedure is repeated until the remaining data are exhausted.

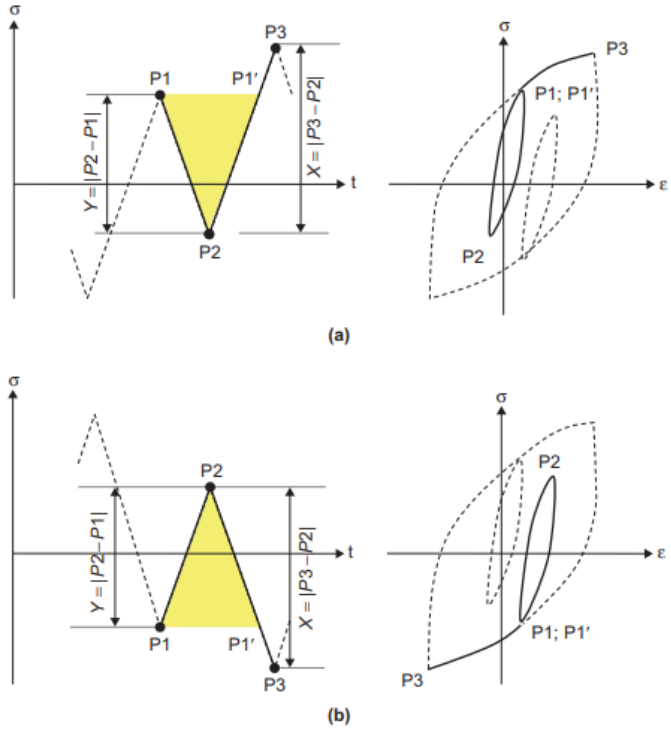


**Figure 2.6 – The three-point rainflow cycle counting rule: (a) Hanging cycle, (b) Standing cycle. Adapted from [47].**

Similar to the three-point counting method, the four-point counting method can be implemented for real-time cycle counting in a non-periodic loading history. This method excludes the contribution of unrepaired reversals and can only recognize closed cycles for fatigue analysis, thus distinguishing from the previous method. The four-point method is illustrated in Figure 2.7.

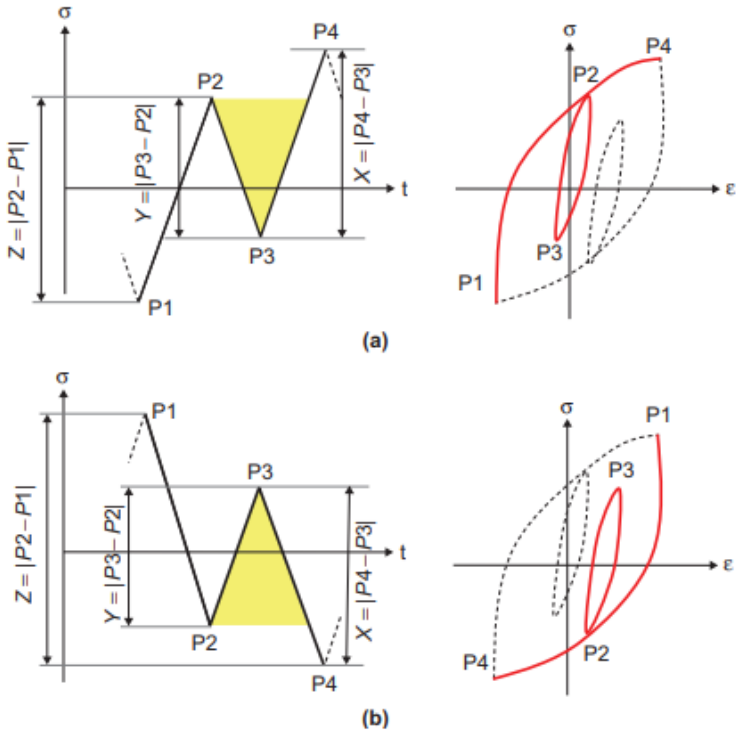


**Figure 2.7 – The four-point rainflow cycle counting rule: (a) Hanging cycle and (b) Standing cycle. Adapted from [47].**

For a complex multiaxial load time history, there are two cycle counting techniques broadly used for fatigue damage assessment [47]. The first approach, known as the critical plane method, uses the uniaxial cycle counting method to calculate fatigue damage in several planes of the material. The critical plane is the one that accumulates the most damage with the fatigue life being calculated through this plane. On the other hand, the equivalent stress or strain amplitude method is based on the assessment of a complex equivalent loading history. This way, fatigue damage, or life is evaluated from the cycles identified by composing the equivalent history.

# 3. NUMERICAL MODEL

## 3.1. Physical Situation

The numerical tests were performed with a C(T) (Compact-Tension) specimen, as presented in Figure 3.1. The specimen is characterized by its initial crack length, $a_0$, of 15 mm and its width, $W$, of 36 mm. The tests were performed considering plane stress state, where the out of plane stress component is null. Since it is not possible to achieve pure plane stress states, experimentally the thickness of the component is as small as possible, in order to make it predominant. This way, the specimen was conceived with a thickness of 0.1 mm in order to guarantee plane stress conditions.

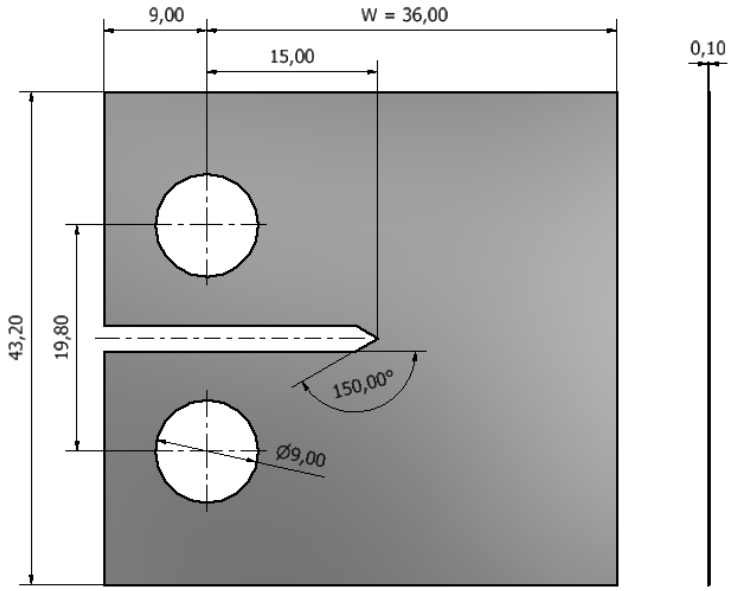


**Figure 3.1 – Physical C(T) specimen. Dimensions in [mm].**

## 3.2. Material

The elastic-plastic behaviour of the materials deeply influences the fatigue process. Thus, it is crucial to describe and predict the elastic-plastic behaviour of metallic materials, in this case through phenomenological constitutive models.

The theory of plasticity can predict the distribution of stresses and strains in polycrystalline metals, not only in situations where the elastic and plastic stresses are of

comparable magnitudes, but also in situations where the plastic stresses are large enough that the elastic stresses are disregarded [51].

These models generally consist of:

- **Yield criterion –** Describes the elastic limit surface under any combination of applied stresses;
- **Hardening law –** Describes the evolution of the elastic limit surface over plastic deformation;
- **Plastic flow rule –** Establishes the relationship between the stress state and the increment of plastic deformation.

The constitutive model is usually described by means of the equivalent stress, $\bar{\sigma}$, which is given by the yield criterion, and the evolution of the yield stress during deformation according to the hardening law, with the geometric factor $Y$.

Thus, the yield is defined through the equilibrium defined in $\mathcal{F}$, given as:

$$\mathcal{F} = \bar{\sigma} - Y \leq 0 \rightarrow \bar{\sigma} = Y. \tag{3.1}$$

The material stress state remains within the yield surface and elastic deformation occurs, when $\bar{\sigma} < Y$. On the other hand, plastic deformation occurs when the associated flow rule states that the increment of the plastic stress tensor is normal to the yield surface, for a stress state such that $\bar{\sigma} = Y$ [38].

For isotropic materials, where the physical properties are constant in all directions, yield criteria such as Tresca and Von Mises are usually adopted. Since the Tresca criterion presents some mathematical difficulties in solving problems due to the existence of angular points on the yield surface, the von Mises criterion emerged. Thus, von Mises' yield criterion was used in this study, defining the material as isotropic.

### 3.2.1. Strain-Hardening Plasticity

Through low cycle fatigue tests, the specimen undergoes successive loadings and unloadings, experiencing plastic deformation, which causing its yield stress to change. This phenomenon, called strain hardening, controls the evolution of the yield strength surface in size, position, and shape when the yield stress is exceeded, through the laws of strain hardening. There are essentially two types of hardening laws, isotropic and kinematic, but there are also hardening laws that are the junction of both.

### Isotropic Hardening

Isotropic strain hardening controls the expansion of the yield surface during plastic deformation, without changes in its initial shape (homothetic expansion), as shown in Figure 3.2. Thus, it is assumed that this surface is defined only by the final plastic stress state, regardless of the actual trajectory [52]. It should be kept in mind that according to this law the material remains isotropic throughout the deformation, while the Bauschinger effect is absent. This effect plays an important role in the presence of cyclic loads, as it allows to characterize the effect of the deformation history in the plastic behaviour.

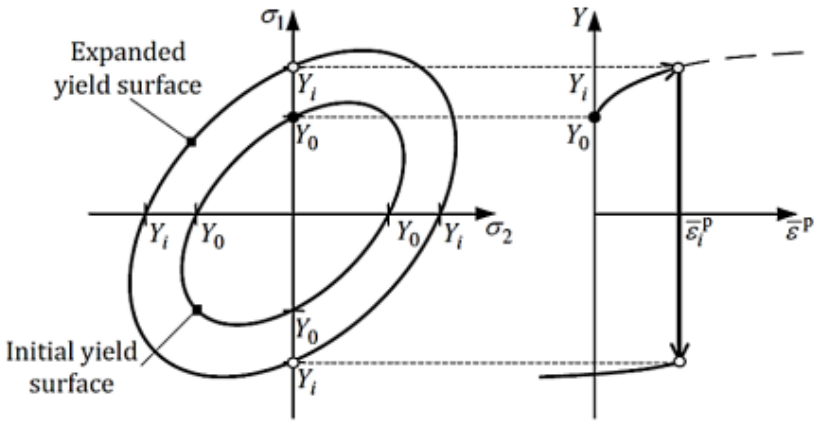


**Figure 3.2 – Representation of the evolution of the yield surface in isotropic hardening, on the left and, on the right side the corresponding stress vs plastic strain curve, adapted from** [53]**.**

Some materials, namely aluminium alloys, the target material of this dissertation, present a phenomenon called saturation stress. To take this phenomenon into account, the Swift [54] model was developed. Swift's law can be written as:

$$Y = K \times (\varepsilon_0 + \bar{\varepsilon}^p)^n, \tag{3.2}$$

where, $K$ and $\varepsilon_0$ are material parameters.

### Kinematic Hardening

Kinematic strain hardening consists in a translation of the yield surface, without changes in its shape and size, as shown in Figure 3.3. Unlike isotropic strain-hardening, kinematic strain-hardening models evidence the Bauschinger effect. This effect consists in the reduction of the yield stress in compression after a tensile load, or vice versa, showing oriented hardening and describing strain paths. The Bauschinger effect takes on special

importance as it shows that the deformation history is relevant to the plastic behaviour of metallic materials.

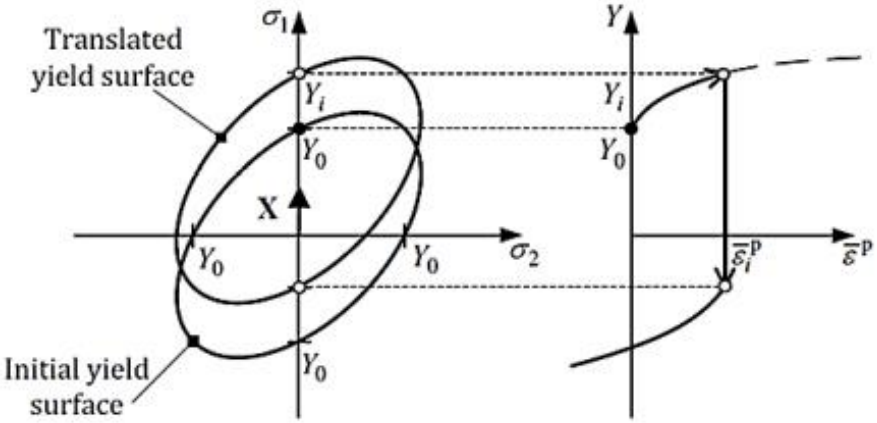


**Figure 3.3 – Representation of the evolution of the yield surface in kinematic hardening, on the left and, on the right side the corresponding stress vs plastic strain curve. Adapted from** [53]**.**

A non-linear kinematic model was proposed by Lemaitre-Chaboche [55], which can be written:

$$\dot{\boldsymbol{X}} = C_{\mathrm{X}}\left[\frac{X_{\mathrm{sat}}}{\bar{\sigma}}(\boldsymbol{\sigma}' - \boldsymbol{X})\right]\dot{\bar{\varepsilon}}^{\mathrm{p}} \; with \; \dot{\boldsymbol{X}}(0) = 0, \tag{3.3}$$

where $C_{\mathrm{X}}$ and $X_{\mathrm{sat}}$ are material parameters and $X$ denotes the back-stress tensor.

This thesis considers an aluminium alloy AA2024-T351 which is widely used in aircraft accessories, gears and shafts, screws, watch parts, computer parts, couplings, fuse parts, hydraulic valve bodies and cryogenic containers. The AA2024-T351 alloy is a high strength material of adequate workability, can be hardened after heat treatment, has good machinability and good surface finish.

The properties of this aluminium alloy were obtained by calibrating numerical stress-strain curves with experimental ones [56]. The experimental results for hysteresis cycles were obtained from low cycle fatigue tests. Table 3.1 shows the material parameters of this alloy.

**Table 3.1 – Material parameters of the material under study** [56]**.**

| **Material** | $\boldsymbol{E}$ **[GPa]** | $\boldsymbol{\nu}$ **[---]** | $\boldsymbol{Y_0}$ **[MPa]** | $\boldsymbol{K}$ **[MPa]** | $\boldsymbol{n}$ **[---]** | $\boldsymbol{C_x}$ **[---]** | $\boldsymbol{X_{\mathrm{sat}}}$ **[MPa]** |
|---|---|---|---|---|---|---|---|
| AA2024-T351 | 72.261 | 0.29 | 288.96 | 389.00 | 0.056 | 138.80 | 111.84 |

## 3.3. Finite Element Model

### 3.3.1. Finite Element Mesh and Boundary Conditions

The mesh used in the numerical tests is shown in Figure 3.4. Note that, because of the CT specimen two symmetric planes, only $^1/_4$ of it was modeled. The model employs 3D linear hexahedral finite elements, with the size of the finite elements being reduced closer to the crack zone. This allows to obtain a greater accuracy of the results, through a refined mesh in the crack path and a lower computational cost due to the outer coarse mesh. At the crack tip, the mesh considers square elements with 8×8 $\mu m^2$, allowing to precisely simulate local strain and stress gradients [57]. In addition, only one finite element layer was used along the thickness.

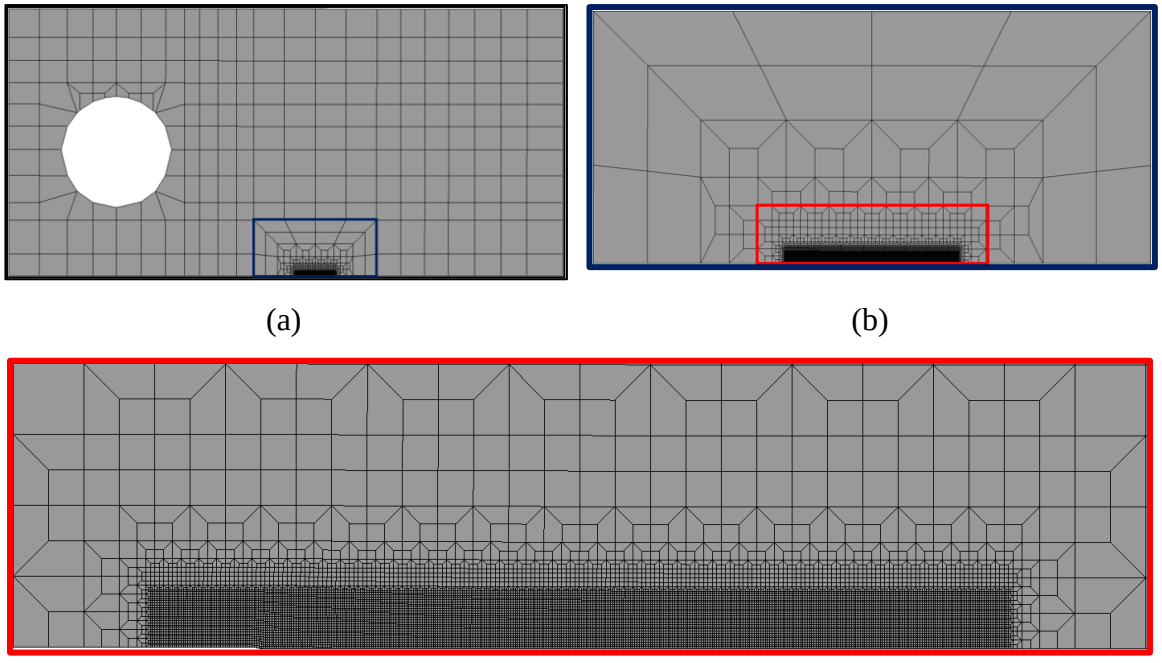

(a) (b)

(c)

**Figure 3.4 – (a) Mesh of the C(T) specimen model; (b) and (c) Details of finite element mesh.**

In this work, the plane stress state is numerically achieved by allowing out of plane displacements in the outer surface, as presented in Figure 3.5. Since only a part of the specimen is presented, the boundary conditions need to be very well defined, as they play a key role in stabilizing the crack tip fields and the level of crack closure. The contact between the flanks of the crack is modelled considering a rigid plane surface aligned with the crack symmetry plane. In some numerical simulations the crack flank contact was removed to

eliminate the crack closure phenomenon. It is important to note that the displacement in the x-axis direction, at the node where the external load is applied is restricted.

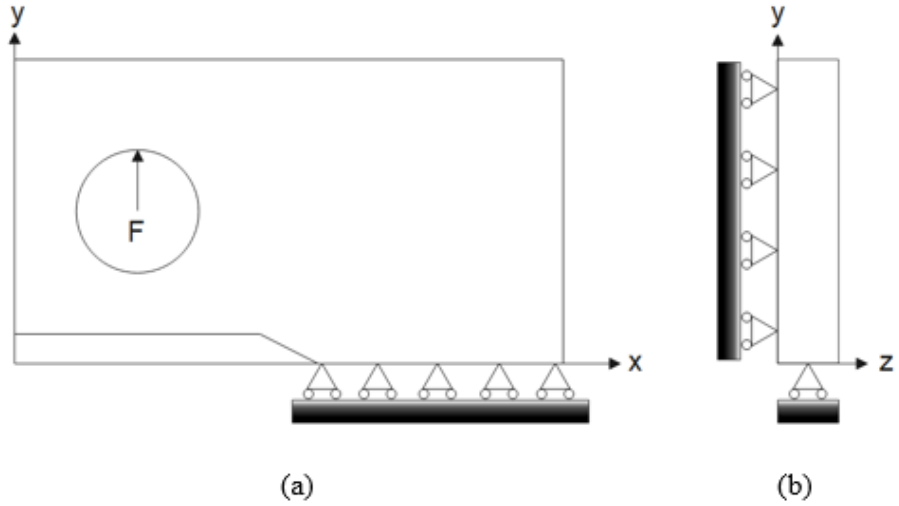


**Figure 3.5 – (a) Model of the C(T) specimen; (b) Boundary conditions for plane stress state.**

### 3.3.2. Crack Propagation

The propagation criterion used in the present study is based on the accumulated plastic deformation at the crack tip. This criterion states that when a critical value of accumulated plastic deformation is reached, the node containing the crack tip is released, i.e., the propagation occurs. Thus, FCG is modelled by releasing the nodes present in the plane of symmetry. Since a node release strategy is followed fatigue is regarded as discrete process, while the physical process is expected to be continuous. The critical value of the accumulated plastic deformation for the AA2024-T351 alloy is of 1.10. This value is considered a material property and was obtained comparing one experimental crack propagation rate and various numerical simulations with different values of critical accumulated plastic strain [56]. It should be noted that this comparison is performed for the same crack length and loading parameters, and it is only necessary to ensure that the crack length of the numerical simulation is in the stabilized regime. The method discussed uses the Total Plastic Strain (TPS) criterion. This criterion considers the cumulative sum of all the plastic strain developed at the Gauss points, even when they do not contain the crack tip [58].

Knowing the distance between nodes (mesh size) and the number of load cycles required to achieve the critical value of accumulated plastic deformation, it is then possible to obtain $da/dN$, which is usually adopted in most literature dealing with constant amplitude loads. Since the present study is focused on variable amplitude loads, the crack propagation

rate is obtained in $da/dt$. This way, knowing the time spent in each cycle it is possible to convert $da/dN$ into $da/dt$. Finally, it is expected to obtain very small crack propagation rates, making necessary to perform many loading cycles to obtain a considerable crack propagation length and, therefore, stabilized $da/dt$ and plastic strain values. This is the crack closure and yield surface expansion and translation require some propagations to stabilize.

### 3.3.3. Load Patterns

The specimen was subjected to four different load patterns, as shown in Figure 3.6. The Low Frequency and the High Frequency loads are constant amplitude loads (CAL). The Low Frequency loading ranges from 6 N to 60 N. On the other hand, the High Frequency load varies only from 6 N to 21 N. Christmas Tree (15-9) and Christmas Tree (9-3) are both variable amplitude loadings (VAL), ranging from 6 N to 60 N. The load pattern Christmas Tree (15-9) is defined during the global increase of the load by increments of +15 N and -9 N. During the global decrease of the load, the pattern contains increments of -15 N and +9 N. The load pattern Christmas Tree (9-3) is defined during the global increase of the load by increments of +9 N and -3 N. During the global decrease of the load, the pattern contains increments of -9 N and +3 N. The difference between these two loadings is that Christmas Tree (15-9) has steeper unloads. A complete cycle of all loading patterns takes 17 seconds, except for the High Frequency pattern, which lasts only 1 second.

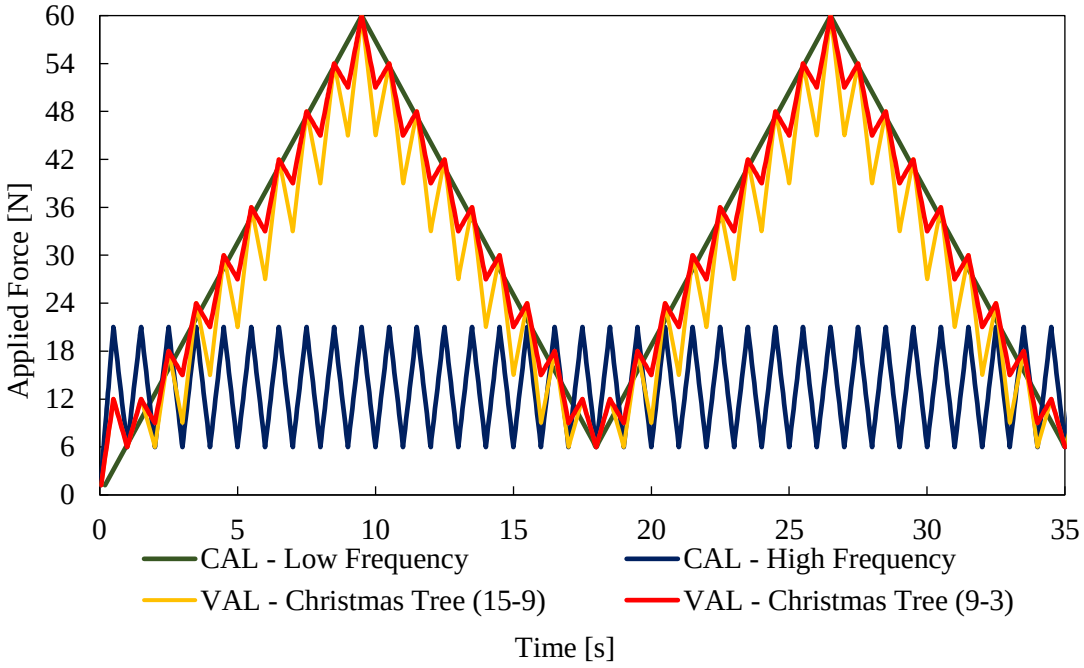


**Figure 3.6 – Four different load patterns used in the numerical simulation.**

## 3.4. Finite Element Software

The FCG numerical analysis was carried out using the in-house finite element code DD3IMP, which was originally developed to simulate sheet metal forming processes [6], [7]. The numerical model considers an elastic-plastic material constitutive model, allowing large deformations and rotations. Furthermore, it assumes that the elastic strains are negligibly small relative to unity.

The typical input files required by the code are presented below.

- **DD3_mesh.msh –** Defines the finite element mesh of the specimen;
- **DD3_materX.dat –** Contains the parameters of the material(s) constitutive laws (Young's modulus, yield stress, parameters of the hardening laws, etc.);
- **DD3_phase.dat –** This file characterizes the loading. Since the loading is defined by force increments, it is necessary to have more than one file of this type, even when the load amplitude is constant;
- **DD3_bcon.dat –** Imposes the boundary conditions on the specimen;
- **DD3_input.dat –** Contains all the numerical parameters, such as the convergence criteria, maximum number of iterations and tolerances, among others;

- **DD3_tool.dat –** Defines the parametric surfaces;
- **DD3oCYCLIC.dat –** Selects the propagation criterion to be used in the numerical simulation, as well as the critical value of the plastic deformation.

The output files contain the simulation results, and the generated files are as follows:

- **R_Line1_CTOD.DD3** and **R_line2_CTOD.DD3 –** Displays the value of CTOD at one and two nodes behind the crack tip, respectively;
- **R_NODESreleased.DD3 –** This file presents a list of all propagations that occurred throughout the simulation, the loading cycle in which the propagation occurred, as well as the plastic deformation at the crack tip nodes;
- **R_TIP.DD3** – Provides information about the stress and strain state in the node containing the crack tip, through all the increments of the simulation;
- **ToolBCIDx.res** and **ToolBCIDy.res** – Displays displacements and forces of the parametric surfaces;
- **Tool_Sym.res –** Presents the contact forces at the crack flanks.

# 4. NUMERICAL RESULTS AND DISCUSSION

In this chapter, the obtained numerical results are presented and discussed for the different analyses. For each one the results of the simulations with and without (penetration allowed) crack flank contact is presented. At the end of each analysis, there is a discussion over results.

## 4.1. FCG Rate

Figure 4.1 presents the crack propagation rates of the 4 load patterns studied, considering contact between the crack flanks, and therefore, crack closure. The value of $da/dt$ increases at the beginning, with a peak occurring after about 500 cycles for the VAL patterns, close to 1600 cycles for the High Frequency pattern, and about 30 cycles for the Low Frequency pattern, at a crack length of about $15.11\ \text{mm}$. Then, the value of $da/dt$ starts a downward behaviour until it stabilizes. Except for the High Frequency, all loading patterns stabilize at a crack growth rate of about $0.19\ \mu\text{m/s}$ for values of crack length greater than $15.30\ \text{mm}$. The High Frequency pattern does not exhibit the same initial peak, stabilizing very quickly. For this reason, the number of crack propagations for this simulation is relatively smaller. Finally, in this loading case the stable value of $da/dt$ is about $0.07\ \mu\text{m/s}$, i.e., about 3 times smaller than the other patterns.

Note that the number of load cycles required to achieve a crack length of $15.30\ \text{mm}$ for both Christmas Tree patterns is about 1400 cycles, while the Low Frequency pattern requires only around 90 cycles.

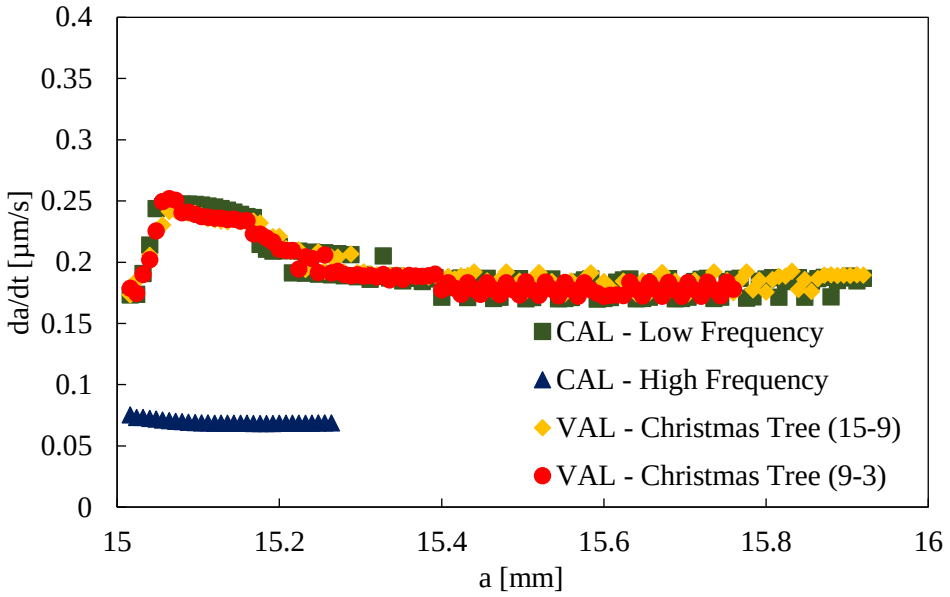


**Figure 4.1 – $da/dt$ in terms of the crack length, $a$, for the various applied loads from the simulations with contact.**

Figure 4.2 shows the propagation rates for the 4 load patterns considering no contact between the crack flanks. The $da/dt$ curves of these load patterns behave similarly to contact load patterns (see Figure 4.1). However, non-contact loading patterns show a more pronounced initial increase, and their stabilization value tends to increase linearly along the crack length. Note that, although the value of $da/dt$ also increases linearly, along the crack length in the simulations with contact, this is less evident, when comparing with non-contact results. Indeed, $da/dt$ increases because during propagation the crack length gets larger and larger, which implies a growth of the magnitude of crack tip fields, and so of the stress intensity factor and propagation rate. Finally, here the overall values of $da/dt$ are superior to those obtained in the simulations with contact, where the stabilization value is $0.33\ \mu m/s$ as the protective effect provided by crack closure is not present. Similarly, to Figure 4.1, the High Frequency loading is also an exception, presenting a $da/dt$ value of about $0.08\ \mu m/s$, this is, around 4 times lower than the other load patterns.

The number of cycles required to reach a crack with 15.30 mm differs from the number of cycles required, to achieve the same length, in the simulations with contact. Without contact, for the Christmas Tree patterns, about 1000 cycles are required. On the other hand, the Low Frequency pattern needs only 70 cycles, the lowest number of cycles. For the High Frequency pattern only 3200 cycles are needed while with contact about 3700 cycles are required. In conclusion, fewer load cycles are needed in the non-contact simulations to

achieve the same crack length and, consequently, higher propagation rates are verified. Note that, the oscillations that the Low Frequency pattern presents are caused by the very high value of $\Delta K$. Although the $\Delta K$ of the VAL patterns also presents high values, the crack propagation on these patterns can occur for different values of force, which tends to reduces the oscillations in a node release strategy. This is contrary to what happens with the Low Frequency pattern, where propagation always occurs at the minimum value of the load cycle. This fact is related to DD3IMP code itself.

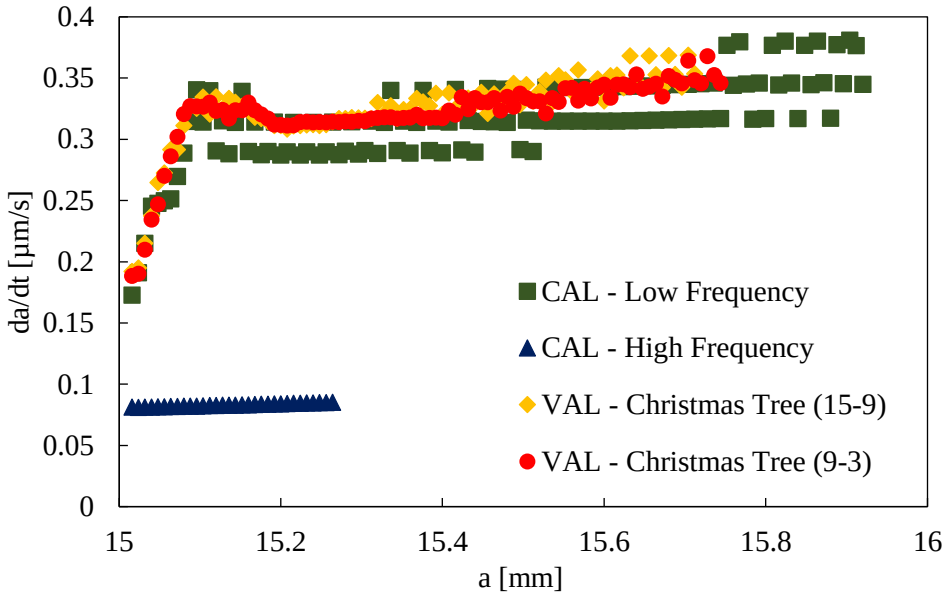


**Figure 4.2 – $da/dt$ in terms of the crack length, $a$, of the various applied loads for the non-contact simulations.**

## 4.2. CTOD

Figure 4.3 presents a typical CTOD curve, obtained at the node behind the crack tip during one load cycle. Results show that the crack remains closed between points A and B, despite the increase in load. The crack opening occurs only when point B is reached. Between B and C, there is a linear increment with load, which is linked to the linear elastic behaviour of the crack. The extrapolation of this linear regime to the maximum load gives, the elastic CTOD, $\delta_e$. The transition to elastic-plastic behaviour occurs at point C. The plastic CTOD increases progressively until point D, where it reaches its maximum value, corresponding to the maximum load. Then the load decreases, and between points D and E a linear relationship is observed. Finally, as the load keeps decreasing the crack closes when the CTOD reaches a null value, at point F.

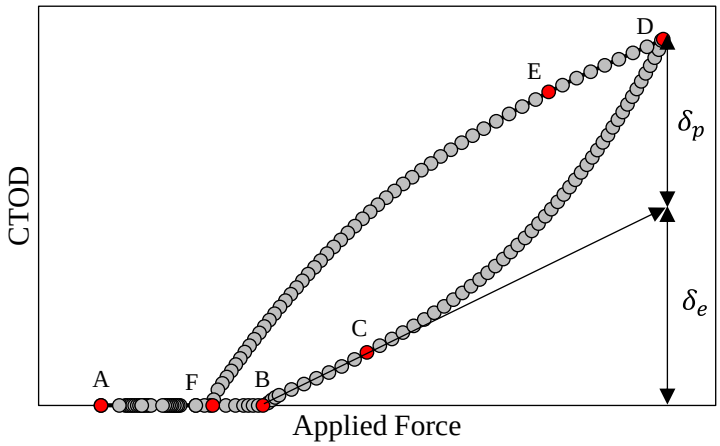


**Figure 4.3 – Representation of CTOD versus applied force in simulations with contact.**

As mentioned before, the CTOD was measured at the node just before the crack tip, i.e., 8 µm behind the tip. This analysis was performed for several distinct crack lengths in order to follow the crack behaviour. Each analysis has a crack length increment of about 0.1 mm between them, starting at the point where the $da/dt$ starts to stabilize ($a = 15.30$ mm). Results show that the evolution of the CTOD during the crack propagation is negligible (slight increase), as shown in Appendix A. This way, the first crack length, $a = 15.30$ mm, was used as point of comparison between load patterns.

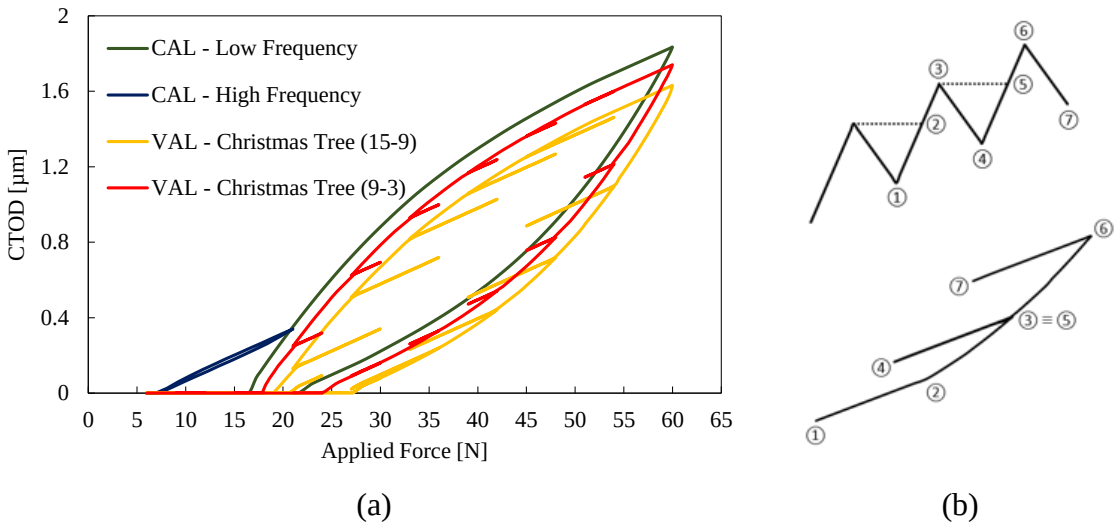


(a) (b)

**Figure 4.4 – (a) Comparison of CTOD curves for the point $a = 15.30$ mm in simulations with contact; (b) Schematic representation of the CTOD curve corresponding to 2 cycles of load on load of the Christmas Tree (15-9) pattern.**

Figure 4.4 (a) shows the evolution of the CTOD curves for a crack length of 15.30 mm, comparing the four studied load patterns. The CTOD curves of the Christmas Tree patterns contain a kind of knurling. This phenomenon occurs due to load pattern

successive loadings and unloadings. Note that in Figure 4.4 (b) is shown a schematic representation of the path of the CTOD curve corresponding to 2 load cycle on load of the Christmas Tree (15-9) pattern. Since each unloading stage of the Christmas Tree (15-9) pattern is steeper, the knurling on the CTOD curves is also steeper. The crack opening load is higher in the Christmas Tree (15-9) pattern because the serration of this load pattern is more pronounced. The Low Frequency pattern shows the highest CTOD of all simulations. Additionally, it presents very similar elastic and plastic CTOD values, with values 1.83 μm and 1.84 μm, respectively. As expected, the High Frequency pattern has the lowest CTOD. Furthermore, this curve is extremely narrow, because the elastic CTOD ($\delta_e = 0.64$ μm) is much higher compared to the plastic CTOD ($\delta_p = 0.04$ μm). Indeed, here the value of the elastic CTOD is about 16 times higher than the plastic CTOD.

The typical CTOD curve obtained through a non-contact simulation differs from the one obtained with a contact simulation, as shown in Figure 4.5. The non-contacting situation is not physically obtainable, only numerical studies allow its representation, since there is an overlap of the crack flanks at minimum load, which cannot occur in a physical specimen. Here, the crack tends to open from the minimum load, unlike what happens in Figure 4.3. Points A and B are coincident and analogously to Figure 4.3, point C corresponds to the transition between the elastic and elastic-plastic regime. Point D corresponds to the maximum load, where the elastic and plastic deformation are maximum. As in Figure 4.3, when the load starts to decrease a linear elastic relation is observed until point E is reached. Due to the reversed plastic deformation after point E, a nonlinear relationship typical of the elastic-plastic regime can be obtained. Note that without crack flanks contact, point F does not exist because there is no crack closure. Finally, the non-contact CTOD curves have a negative part, which corresponds to the penetration of the flanges when the load is close to the minimum.

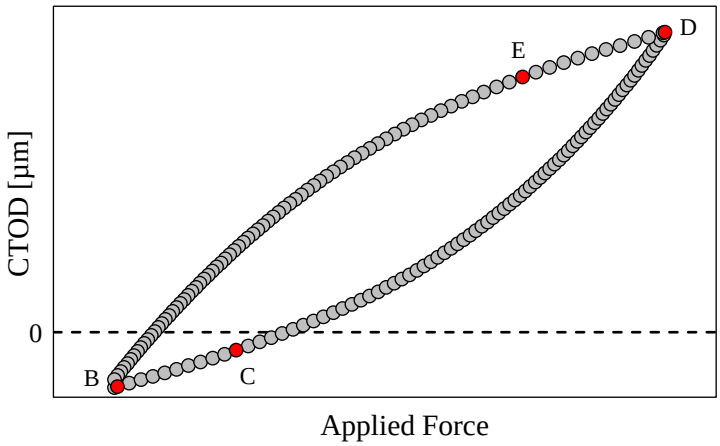


**Figure 4.5 – Representation of CTOD versus applied force in non-contact simulations.**

Appendix B presents the comparison between the distinct crack length analysed in each pattern, except for the Christmas Tree (15-9) simulation. This way, the first crack length, $a = 15.30$ mm, was used as point of comparison between load patterns because the evolution of the CTOD during the crack propagation is negligible, as shown in Appendix B. In Christmas Tree (15-9) pattern, the behaviour of the CTOD at the various points along the crack length has a different behaviour, that is, the graphs have undergone translations between them, as presented in Figure 4.6.

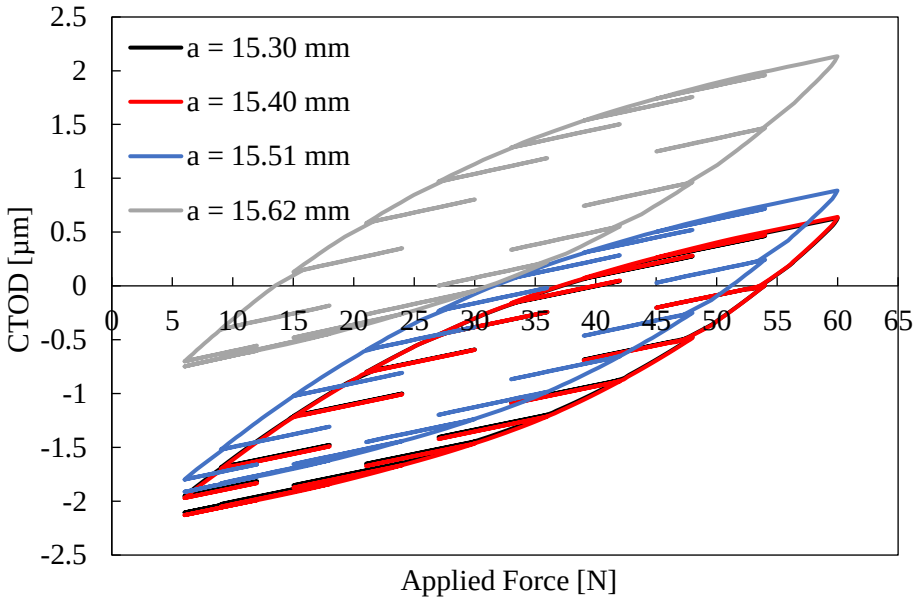


**Figure 4.6 – Effect of crack length on CTOD curves for the Christmas Tree (15-9) simulation without contact.**

The first two crack length values analysed ($a = 15.30$ mm and $a = 15.40$ mm) have almost coincident CTOD curves. Then, at point $a = 15.51$ mm, the CTOD shows a slight

translation of about 0.25 µm in the upward direction. Also, the CTOD curve at $a = 15.62$ mm shows a translation relative to point $a = 15.51$ mm of about 1.29 µm. In order to verify the reasons for the occurrence of this phenomenon, a more detailed analysis was performed around $a = 15.40$ mm and $a = 15.62$ mm. This way, the behaviour of the CTOD curves, immediately before and after a propagation cycle was analysed, as shown in Figure 4.7 (c) and (d). Additionally, Figure 4.7 (a) and (b) present the respective propagation instants along the load blocks.

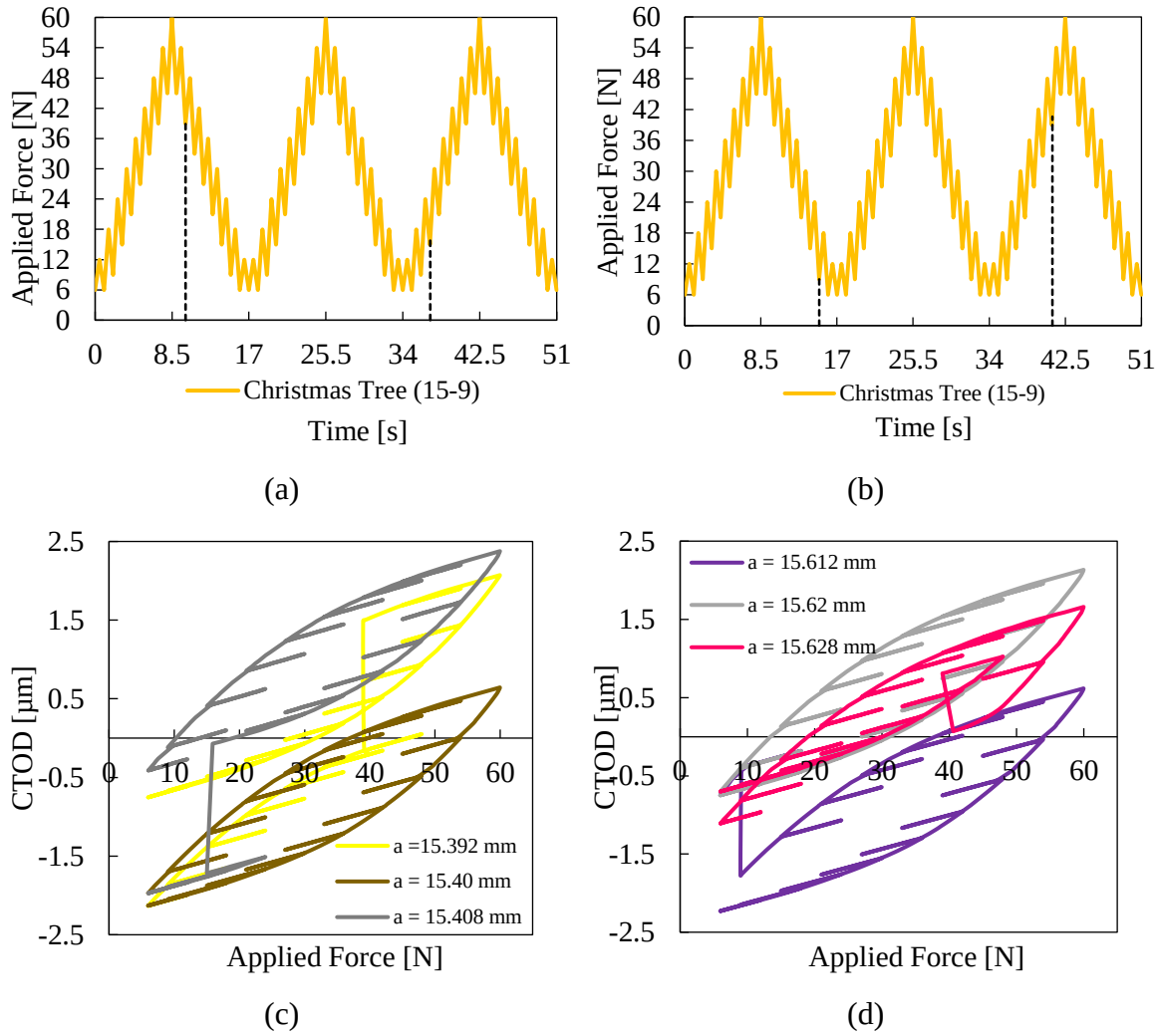


**Figure 4.7 – Christmas Tree (15-9) loading cycles around: (a) $a = 15.40$ mm; (b) $a = 15.62$ mm; CTOD curves corresponding to the Christmas Tree (15-9) loading cycles around: (c) $a = 15.40$ mm; (d) $a = 15.62$ mm.**

Note that a load block of the VAL patterns consists of 17 load cycles. The CTOD curves are discontinuous between two consecutive load blocks, causing vertical displacements of the curves, with no distortion of their shape. This phenomenon occurs because the crack propagation can occur at any time of the load block. This way, the crack

propagation may not occur at the global minimum load of the load block but at the local minimum of at load cycle, at higher load values. The first vertical dotted line in Figure 4.7 (a) corresponds to the crack propagation from a value of $a = 15.392$ mm to $a = 15.40$ mm, while the second dotted line is the crack propagation from $a = 15.40$ mm to $a = 15.408$ mm. Analogously, this phenomenon happens at point $a = 15.62$ mm, in Figure 4.7 (b). Note that this phenomenon also occurs for the loading of the Christmas Tree (9-3).

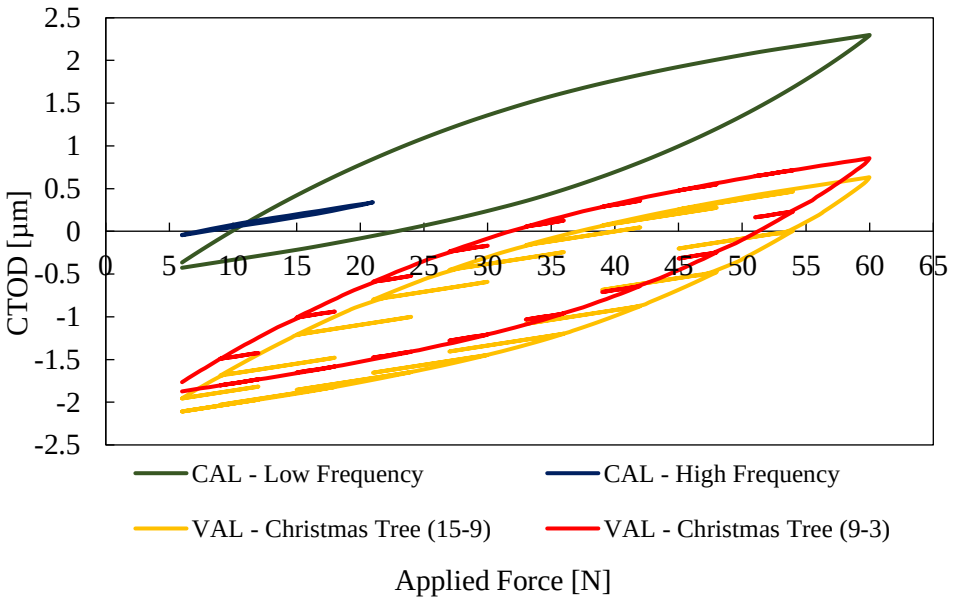


**Figure 4.8 – Comparison of CTOD curves for the point $a = 15.30\ mm$ in non-contact simulations.**

The comparison of the non-contact CTOD curves, between the various patterns is shown in Figure 4.8. The shapes of the CTOD curves are identical to the curves obtained with contact. Note that, the CTOD curves of the variable amplitude loadings were obtained after a node release at very low loading. Since the crack propagation did not occur at the minimum load of the load block, a translation of the CTOD curves of the VAL patterns occurred, as in Figure 4.6 and Figure 4.7 (c).

## 4.3. Plastic Strain

Figure 4.9 presents the evolution of the plastic strain, evaluated at the node containing the crack tip, during some node releases starting at a crack length, $a = 15.30$ mm. Different load patterns are compared. Results show that the plastic strain value, at the beginning of each new propagation, is approximately 0.8 for all load patterns, except for the High Frequency one. Indeed, in High Frequency after each propagation, the node that receives the

crack tip has null plastic strain value. This indicates that due to relatively low load range, only the element at the tip is accumulating plastic deformation. Thus, to reach the critical plastic deformation value of this material, ($\bar{\varepsilon}_c^p = 1.10$) the High Frequency pattern requires the largest accumulation of plastic strain, once the node receives the crack tip, in comparison with the other load patterns. This means, that this pattern needs more load cycles to reach the critical value (assuming the same plastic strain growth rate in all cases). Therefore, the High Frequency pattern has a lower crack propagation rate than the other patterns. Note that the value of critical plastic deformation for the Low Frequency pattern is equal to the other loading patterns. However, this pattern reaches values close to 1.2 because the crack propagation occurs only at the minimum load value.

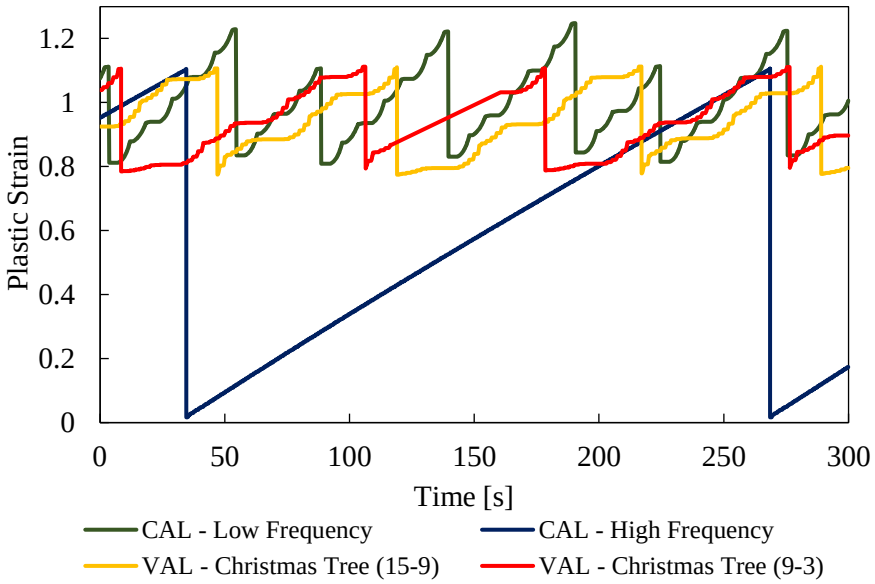


**Figure 4.9 – Comparison of plastic strain curves of the various applied loads from the simulations with contact.**

Figure 4.10 shows the evolution of the plastic strain, evaluated at the crack tip, during some crack propagations for $a = 15.30\,\text{mm}$, comparing different load patterns and neglecting the contact between the crack flanks. Results show that the crack flanks contact reduces the plastic strain accumulation rate, requiring a longer time, in all loading patterns, to reach the critical value of plastic deformation. In fact, this occurs due to the effect of crack closure that protects the material and slows down the accumulation of plastic deformation. The value of plastic deformation at the beginning of each new propagation is approximately 0.8 for both variable load amplitude patterns. For the Low Frequency load pattern, the minimum plastic deformation value is slightly higher, around 0.9. This occurs because the

cumulative plastic deformation in the previous propagation reaches na higher value (~1.2) influencing the minimum plastic deformation for this load pattern.

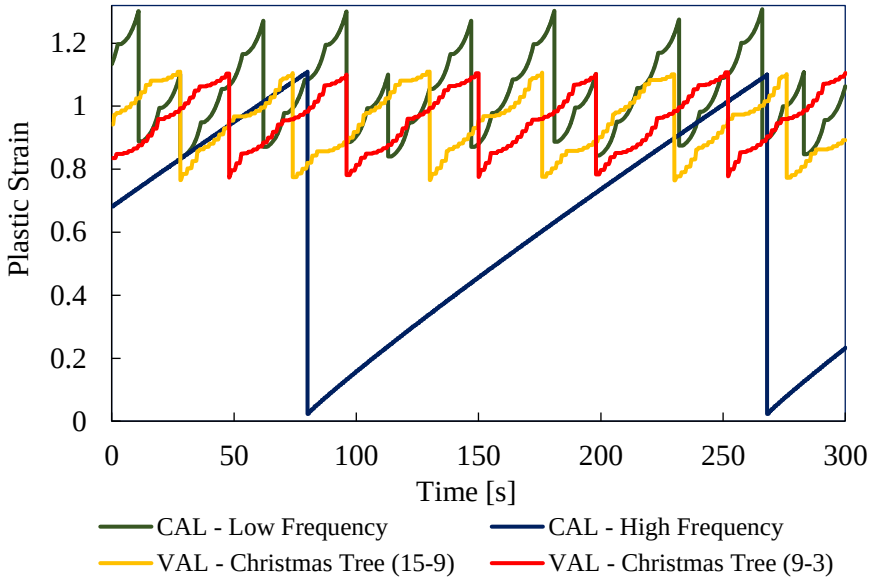


**Figure 4.10 – Comparison of plastic strain curves of the various applied loads from the simulations without contact.**

Figure 4.11 shows the evolution of the plastic strain evaluated at the crack tip for $a = 15.30$ mm, for the different load patterns. In order to compare the behaviour of the increase in plastic deformation during the same time interval, 17 load cycles of the High Frequency pattern were used. As mentioned earlier, for the remaining load patterns, only 1 load cycle is shown in Figure 4.11. Note that the plastic deformation graphs have undergone a translation of both axes, setting both initial plastic strain and time to zero. Considering the constant amplitude loading cases, both present exponential growths of plastic deformation at the crack tip. However, the Low Frequency pattern presents more prominent increases, in comparison to the High Frequency one, due to the also higher $\Delta K$ levels. For both Christmas Tree loadings patterns, the plastic deformation has several increasing steps. These steps occur due to successive loading and unloading phases. The biggest "jump" in the plastic strain occurs at maximum load, for a time of 8.5 s. In conclusion, all loadings have a similar plastic strain growth rate for the same time interval, i.e., plastic strain reaches values close to 0.14 for all simulations considering the same time intervals.

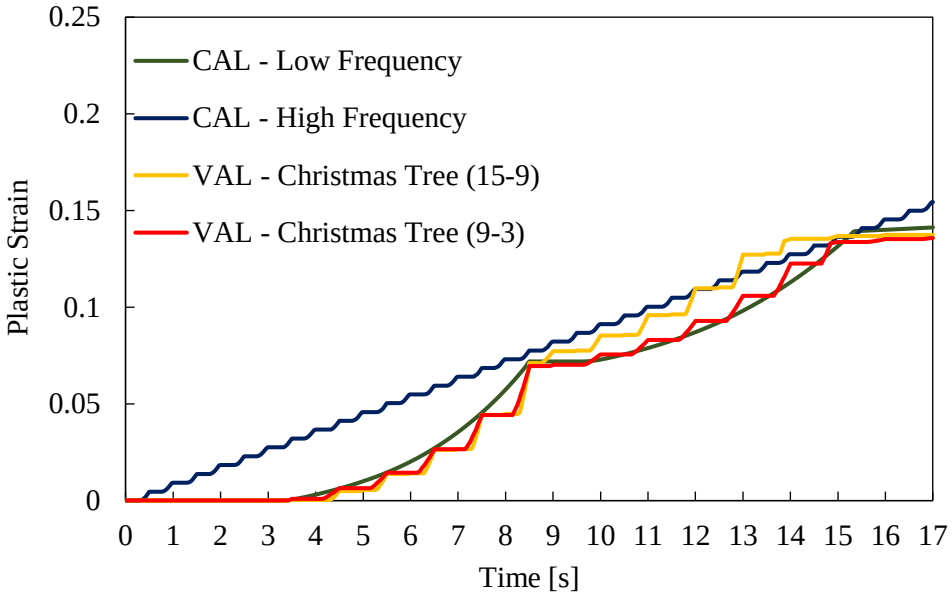


**Figure 4.11 – Comparison of plastic strain evolution for the point $a = 15.30$ mm in contact simulations.**

Figure 4.12 shows the evolution of the plastic deformation evaluated at the crack tip for $a = 15.30$ mm, comparing different load patterns from the non-contact simulations. The plastic strain behaviour, of each simulation has several similarities with the results obtained considering the contact of the crack flanks. Despite the similarities, the crack closure has an important influence on the plastic deformation rise, in VAL and Low Frequency patterns. Nevertheless, the plastic strain growth rate is globally higher for the situation without contact. All plastic strain accumulation curves tend towards the limit value. This is because there is no crack closure phenomenon in the absence of contact.

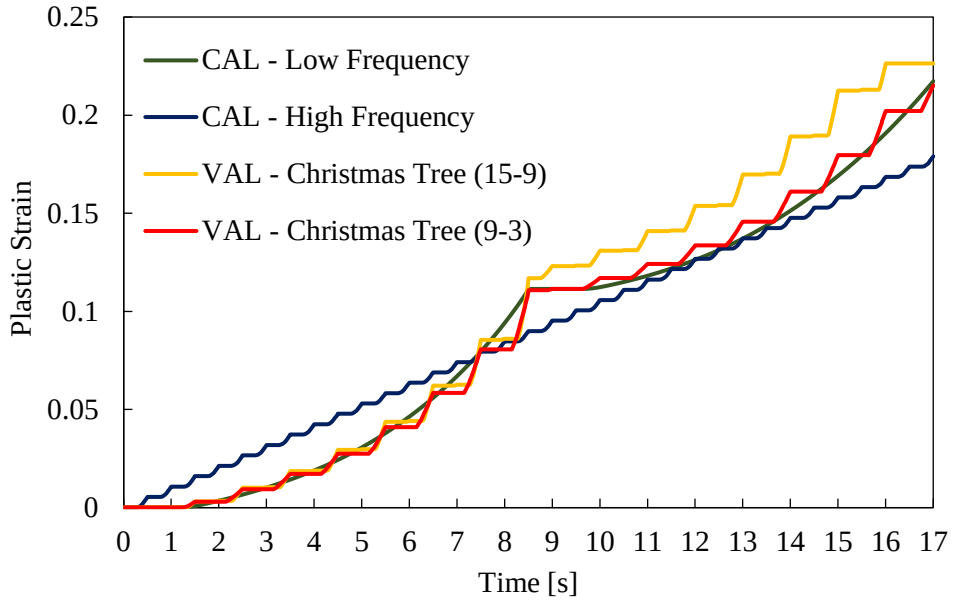


**Figure 4.12 – Comparison of plastic strain curves for the point $a = 15.30$ mm in non-contact simulations.**

### 4.3.1. Constant Amplitude Loading

In order to better understand the effect of the loading patterns on the plastic deformation at the crack tip, the portion of the loading cycle with plastic strain rise was identified. The results are presented, in Figure 4.13, for the constant amplitude loading patterns. Considering the Low Frequency loading pattern (Figure 4.13 (a) and (c)), before the crack opening loading, $F_{\text{open}} = 21.55$ N, there is no plastic deformation. After its opening, it enters in the elastic domain, for about half a second, where is still no plastic deformation. After around 3 s, from the beginning of the load cycle, the plastic deformation increases exponentially until it reaches the maximum load. When the unloading starts, the crack recovers the elastic behaviour and, once again, enters the plastic domain where the plastic deformation increases, also exponentially, until the crack closes, at $F_{\text{closure}} = 16.73$ N. After the crack closure plastic deformation still increases, but with a slight linear behaviour. This is important because it indicates that there is damage below crack closure, and therefore the concept of effective load range is not totally correct.

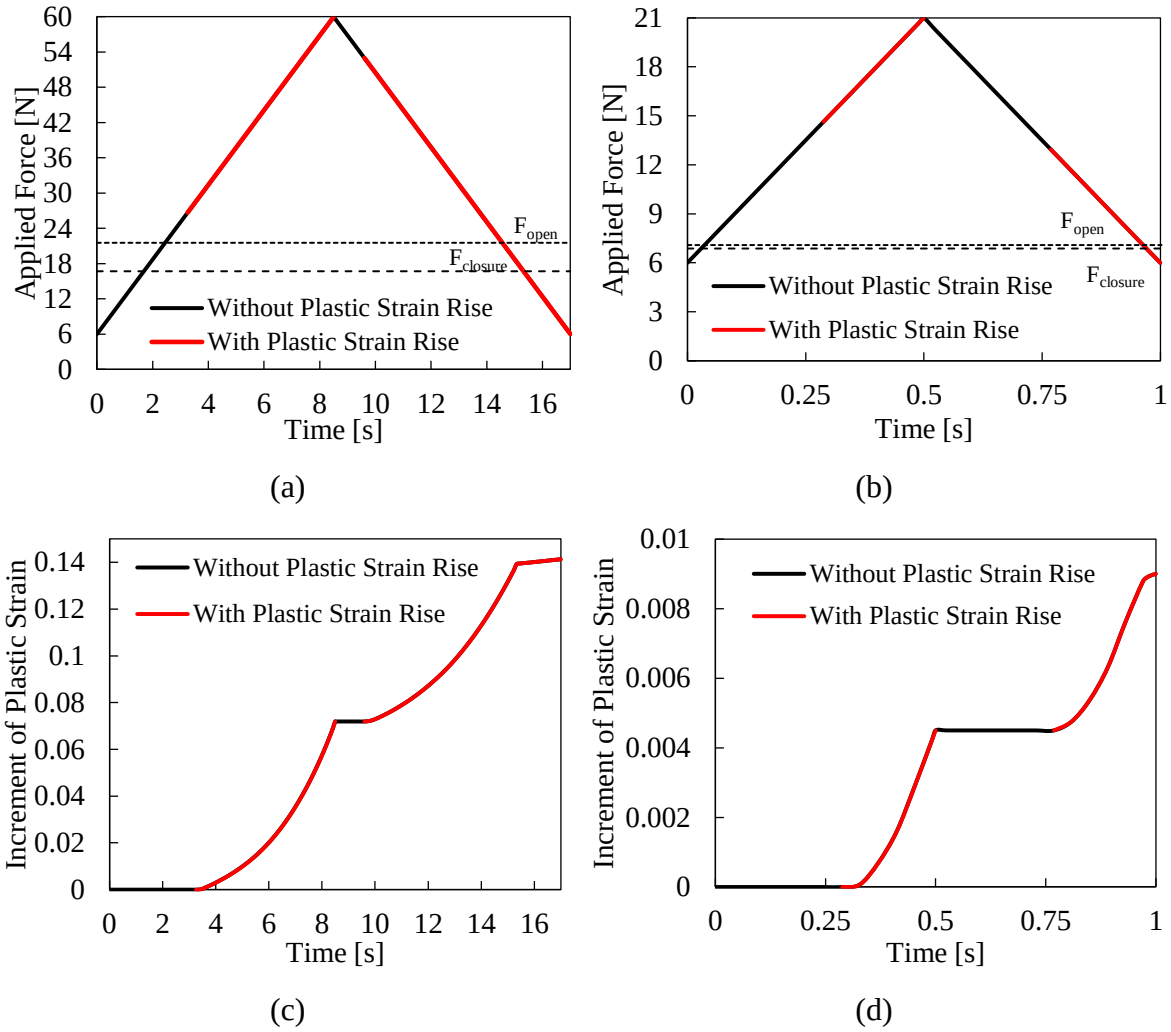


**Figure 4.13 – Evolution of plastic deformation during loading to $a = 15.30$ mm: (a) Low Frequency pattern; (b) High Frequency pattern; Plastic strain rise: (c) Low Frequency pattern; (d) High Frequency pattern.**

In the High Frequency load pattern (Figure 4.13 (b) and (d)), the plastic deformation also increases exponentially. After the crack opening, at $F_{\text{open}} = 7.08$ N, the crack is in the elastic domain and only enters the plastic domain when the loading reaches values close to the peak. When the loading starts to decrease, the crack behaves elastically, as it does with the Low Frequency pattern. The crack again has an increase in plastic deformation, also in an exponential way, when the applied force values reach low values. After the crack closure occurs at $F_{\text{closure}} = 6.88$ N, the plastic deformation continues to increase, but in a less pronounced way. Note that the CTOD of this loading pattern (see Figure 4.4) is predominantly elastic, making the plastic deformation, in this loading, very small. The increase of plastic strain at the crack tip in a single load cycle under the High Frequency load pattern is about 15 times smaller than in the Low Frequency load pattern.

Figure 4.14 shows the constant amplitude loading cycles together with the time intervals where an increase in plastic deformation occurs, without crack flanks contact. As mentioned before, in non-contact simulations, the crack closure phenomenon does not occur. Consequently, the plastic deformation of these loads has a similar behaviour to that observed in Figure 4.13. The increase in plastic strain, in both cases, occurs only exponentially, because there is no linear behaviour in the plastic strain accumulation after crack closure, due to contact absence. Thus, higher values were obtained for the plastic deformation. Furthermore, for these load patterns, the growth of plastic deformation also starts sooner. Although this is more evident in the Low Frequency pattern, in the High Frequency pattern it also happens. This is because the crack opens from the minimum load.

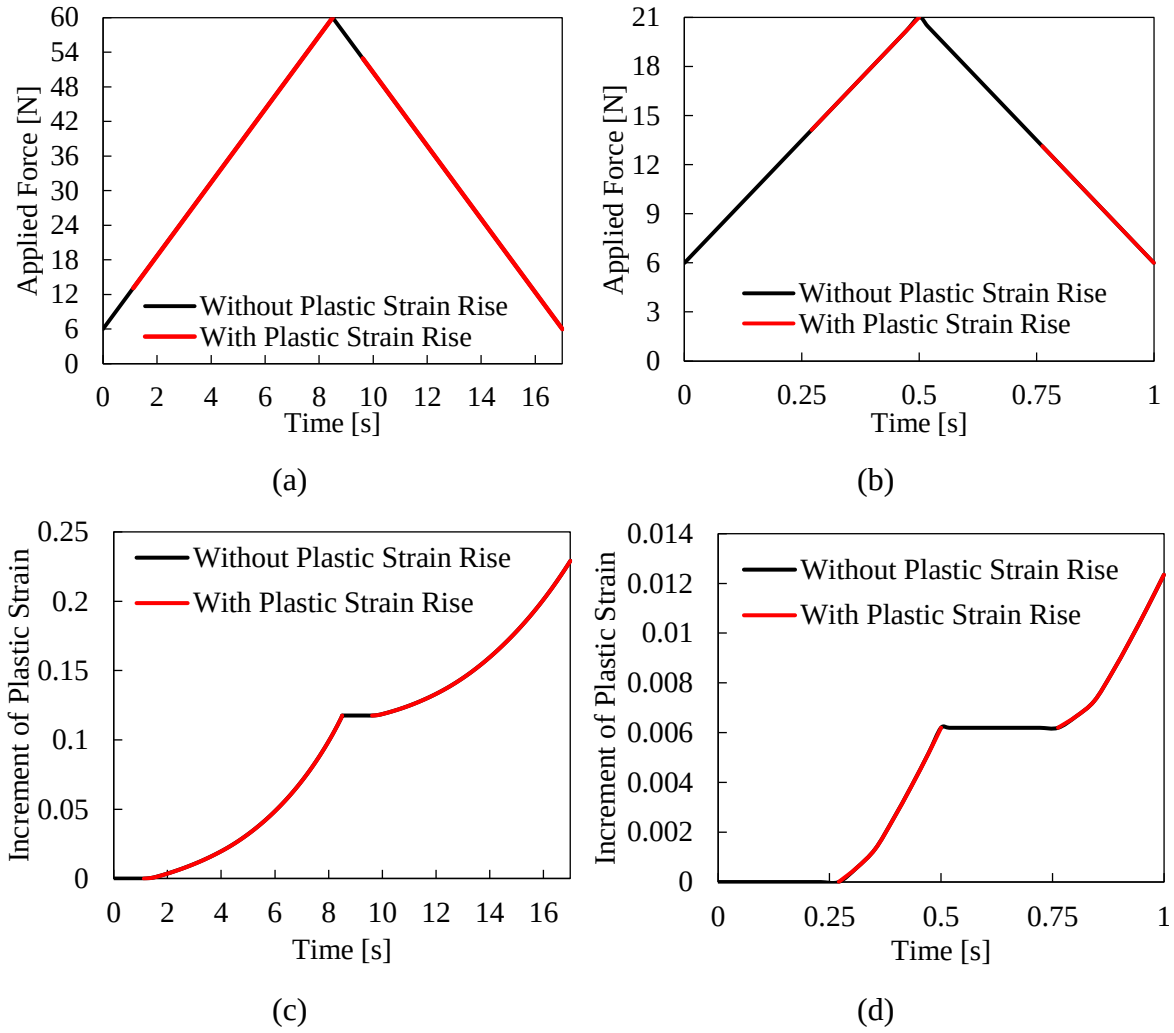


**Figure 4.14 – Evolution of plastic deformation during loading to $a = 15.30$ mm in non-contact simulations: (a) Low Frequency pattern; (b) High Frequency pattern; Plastic strain rise in non-contact simulations: (c) Low Frequency pattern; (d) High Frequency pattern.**

### 4.3.2. Variable Amplitude Loading

Figure 4.15 shows the portion of the Christmas Tree (15-9) and Christmas Tree (9-3) patterns where an increase in plastic deformation occurs. The increase of plastic deformation before the crack opening is negligible for both load patterns. The crack opening load is of $F_{\text{open}} = 27.11$ N in the Christmas Tree (15-9) pattern. For the Christmas Tree (9-3) pattern the crack opening occurs for a value of $F_{\text{open}} = 24$ N. Until the loading reaches overall maximum peak of the load block, plastic deformation occurs essentially at the load cycle peaks. When the loading starts to have global decreasing behaviour, after around 9 s, the plastic deformation starts to manifest itself in the valleys of successive unloadings. Note that plastic strain keeps on increasing, even after crack closes, at $F_{\text{closure}} = 19.13$ N and $F_{\text{closure}} = 17.85$ N for the Christmas Tree (15-9) and Christmas Tree (9-3) pattern, respectively. Nevertheless, after closure, the increase in plastic deformation become much less pronounced than when the crack is open. This, once again, destroys the purity of effective load range, which usually represents the crack closure phenomenon.

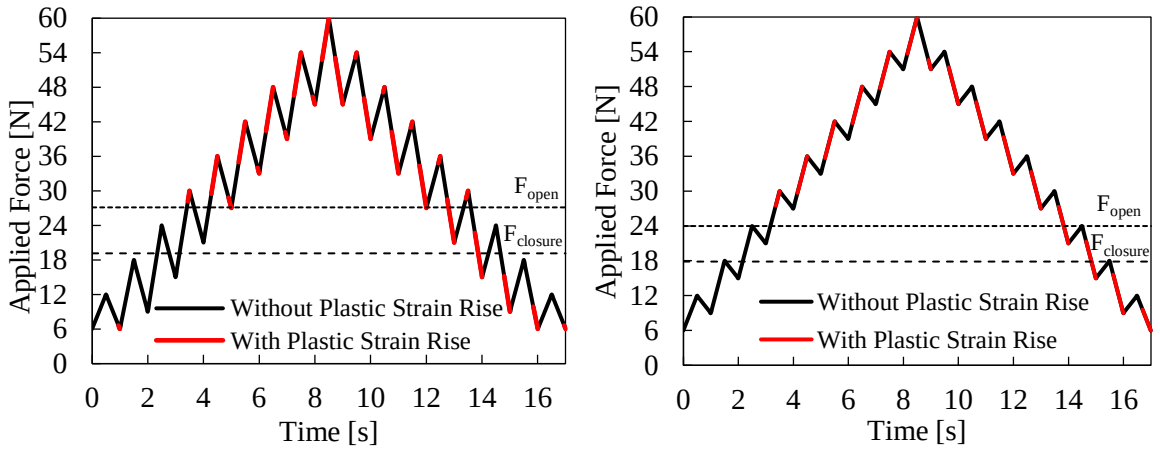

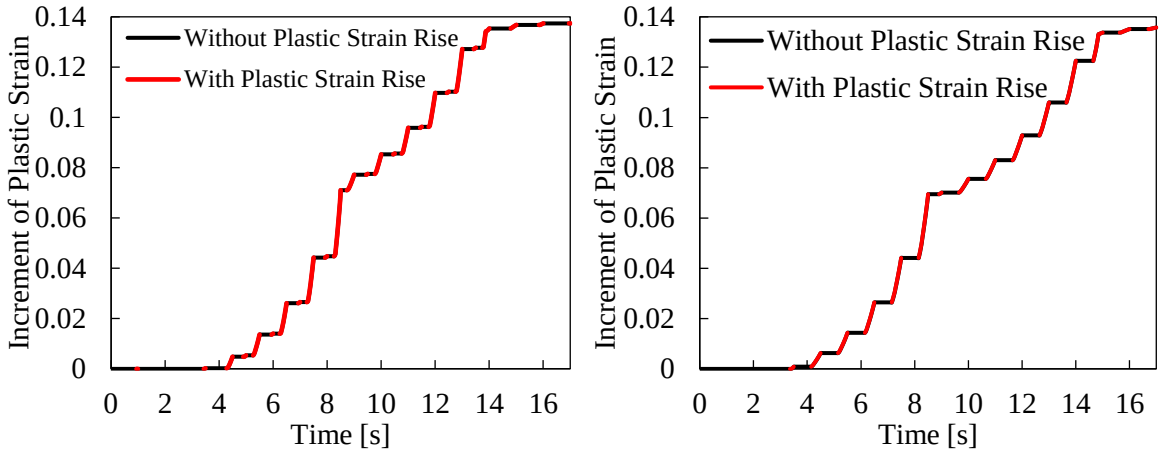


**Figure 4.15 – Evolution of plastic deformation during loading to $a = 15.30$ mm: (a) Christmas Tree (15-9) pattern; (b) Christmas Tree (9-3) pattern; Plastic strain rise: (c) Christmas Tree (15-9) pattern; (d) Christmas Tree (9-3) pattern.**

Figure 4.16 shows the portion of the variable amplitude loading patterns where plastic deformation increases, neglecting the contact between the crack flanks in the simulations. The plastic deformation behaves similarly to what was previously observed in contact simulations (see Figure 4.15). Since the phenomenon of crack closure does not exist, higher values of plastic deformation arise. The growth of plastic deformation is more pronounced, both at the beginning of the loading cycle and at the end.

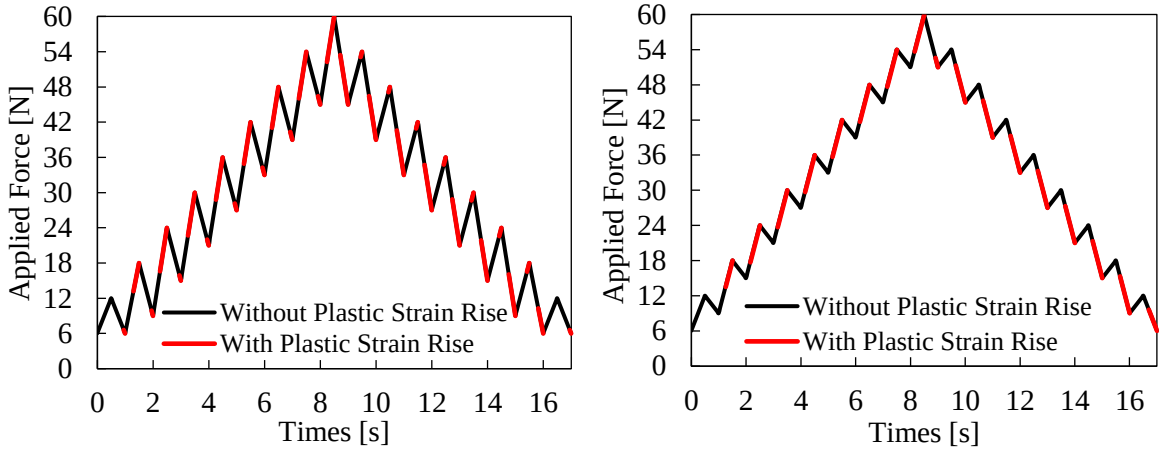

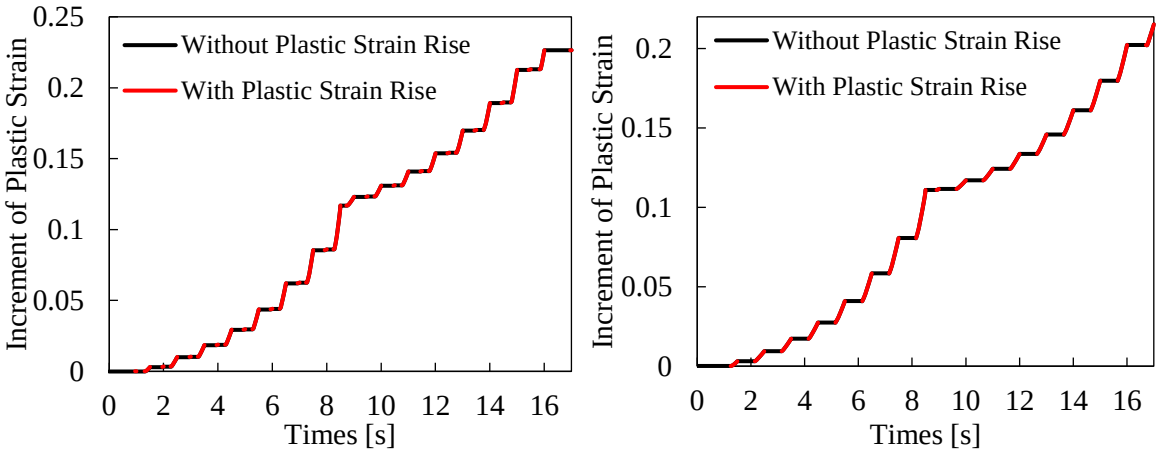


**Figure 4.16 – Evolution of plastic deformation during loading to $a = 15.30$ mm in non-contact simulations: (a) Christmas Tree (15-9) pattern; (b) Christmas Tree (9-3) pattern; Plastic strain rise in non-contact simulations: (c) Christmas Tree (15-9) pattern; (d) Christmas Tree (9-3) pattern.**

## 4.4. Deformed Plastic Zone

### 4.4.1. Constant Amplitude Loading

Figure 4.17 shows the size of the plastically deformed zones, which was identified considering a limit plastic strain of 0.05%, for the constant amplitude load patterns. The size of the plastically deformed zone for the High Frequency pattern is very small compared to the other load patterns. This is because the load range of this simulation is lower than the others (see Figure 3.6). The plastic zone size ahead of the crack tip is of 0.18 mm and 1.42 mm for the High Frequency and Low Frequency loading patterns, respectively, in the crack propagation direction.

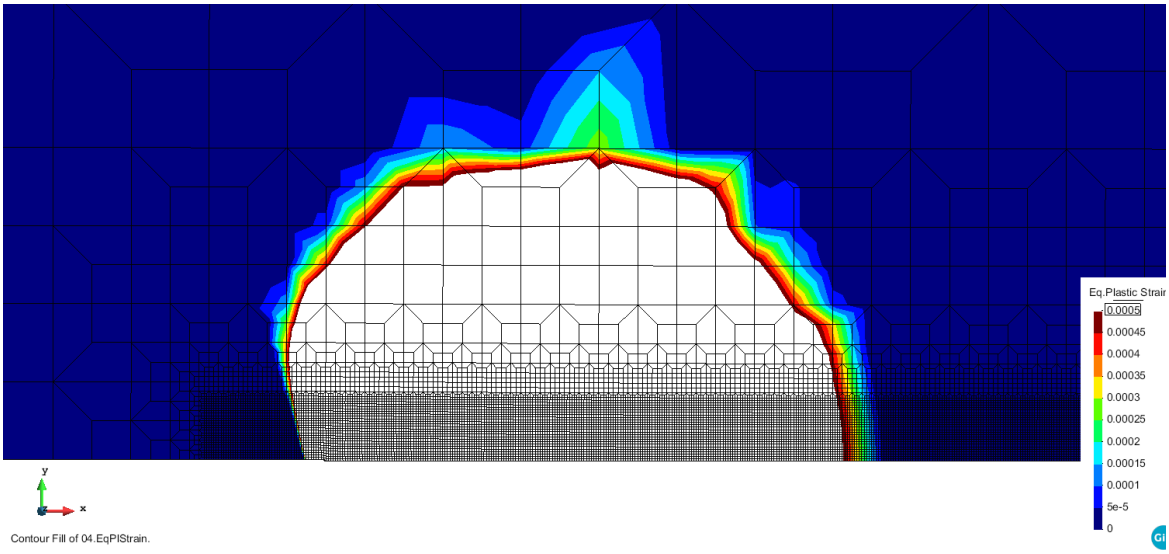


(a)

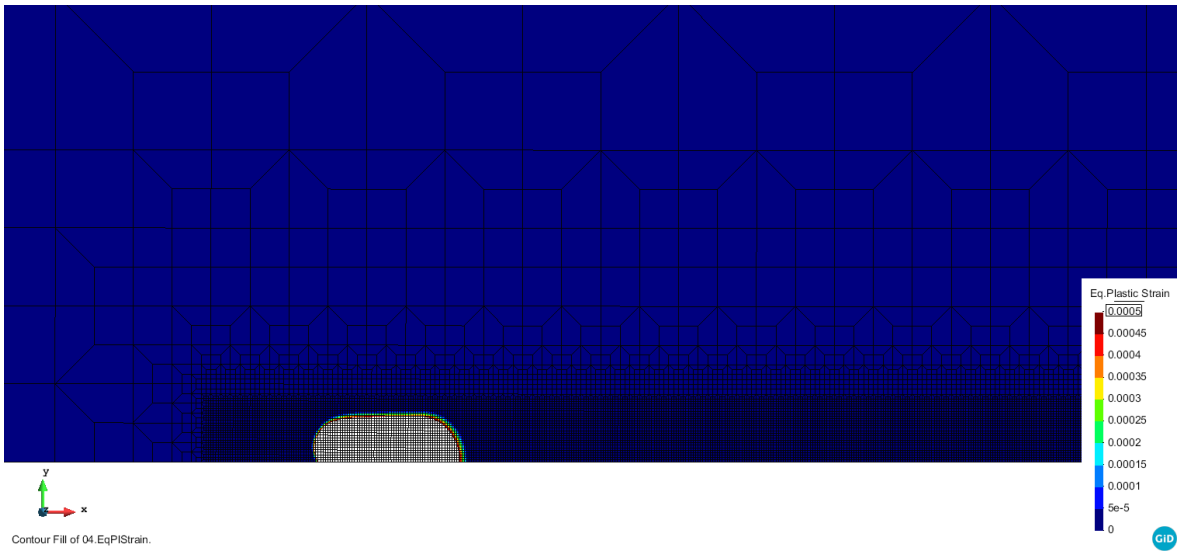


(b)

**Figure 4.17 – Plastically deformed zone for $a = 15.30$ mm: (a) Low Frequency pattern; (b) High Frequency pattern.**

Figure 4.18 shows the size of the plastically deformed zones for the constant amplitude loadings considering no contact between the crack flanks. Although the maximum plastic deformation value is higher near the crack tip, the size of the plastically deformed zone is identical to that of the simulations with contact, as can be seen in Figure 4.17.

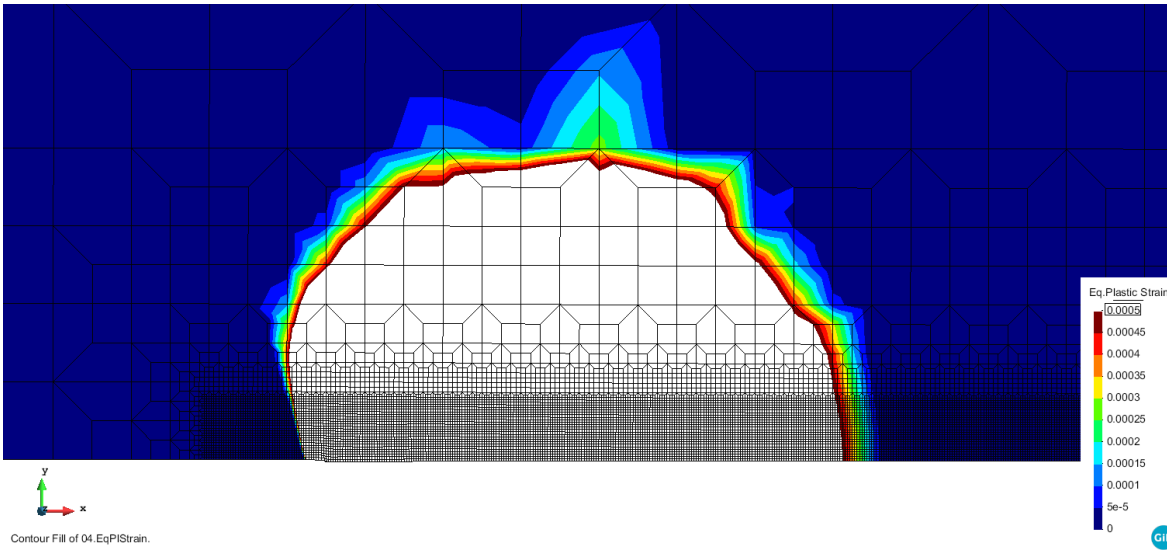


(a)

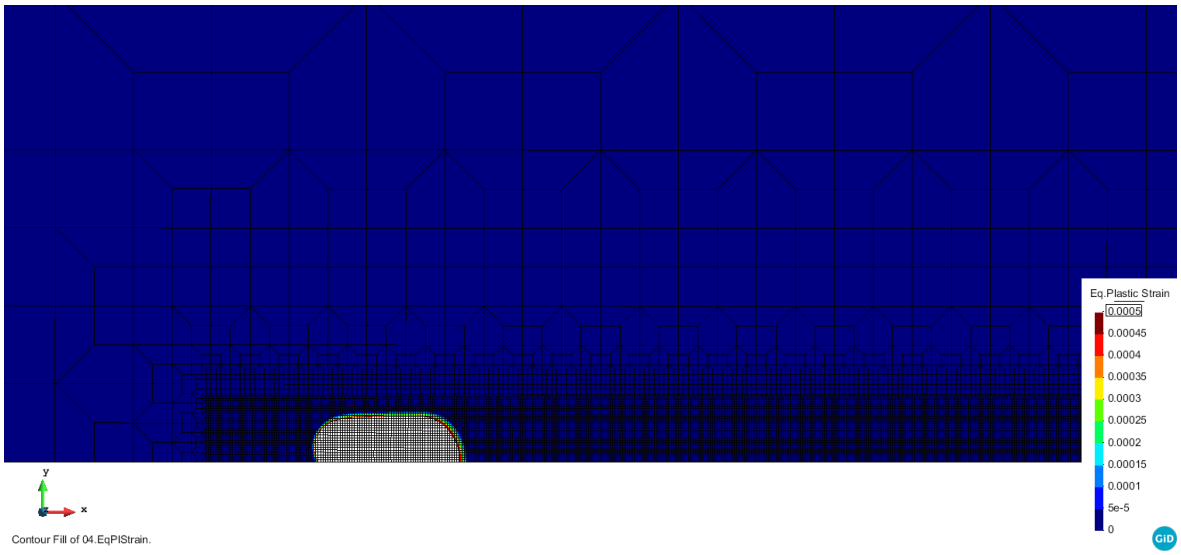


(b)

**Figure 4.18 – Plastically deformed zone for $a = 15.30$ mm in non-contact simulations: (a) Low Frequency pattern; (b) High Frequency pattern.**

### 4.4.2. Variable Amplitude Loading

Figure 4.19 shows the size of the plastically deformed zone for both Christmas Tree load patterns, evaluated for $a = 15.30$ mm. The size of the plastically deformed zone is similar between patterns, which was expected since the plastic deformation level tends to the same value (see Figure 4.11) and the crack propagation rates are identical (see Figure 4.1). Moreover, the Christmas Tree patterns has a deformed zone similar those obtained in the Low Frequency pattern due to the same load range. In fact, the monotonic plastic zone

is obtained at the maximum load of the load block, which is the same for Low Frequency and Christmas Tree load patterns.

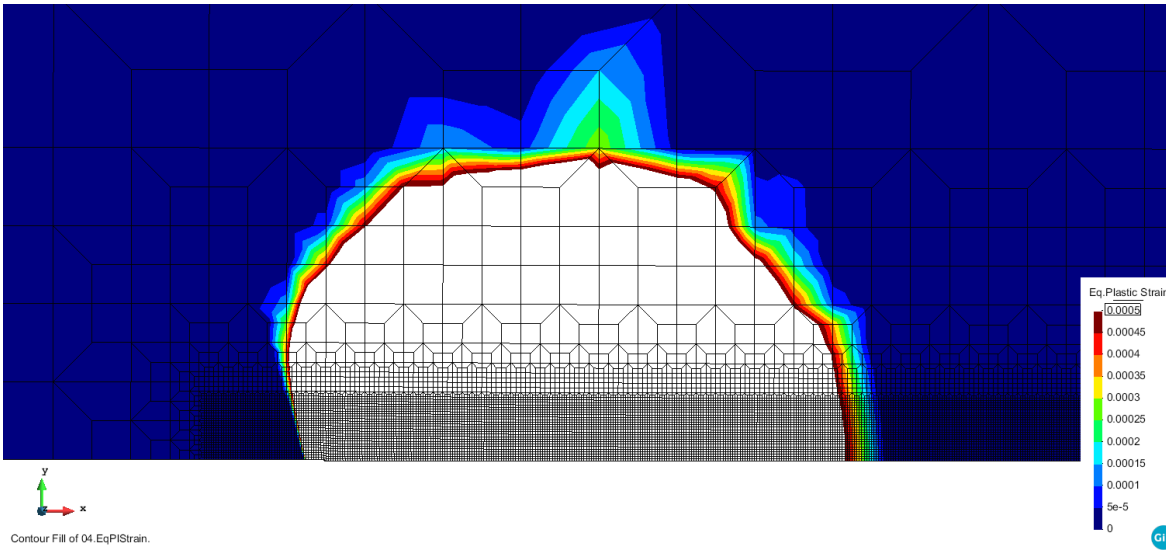


(a)

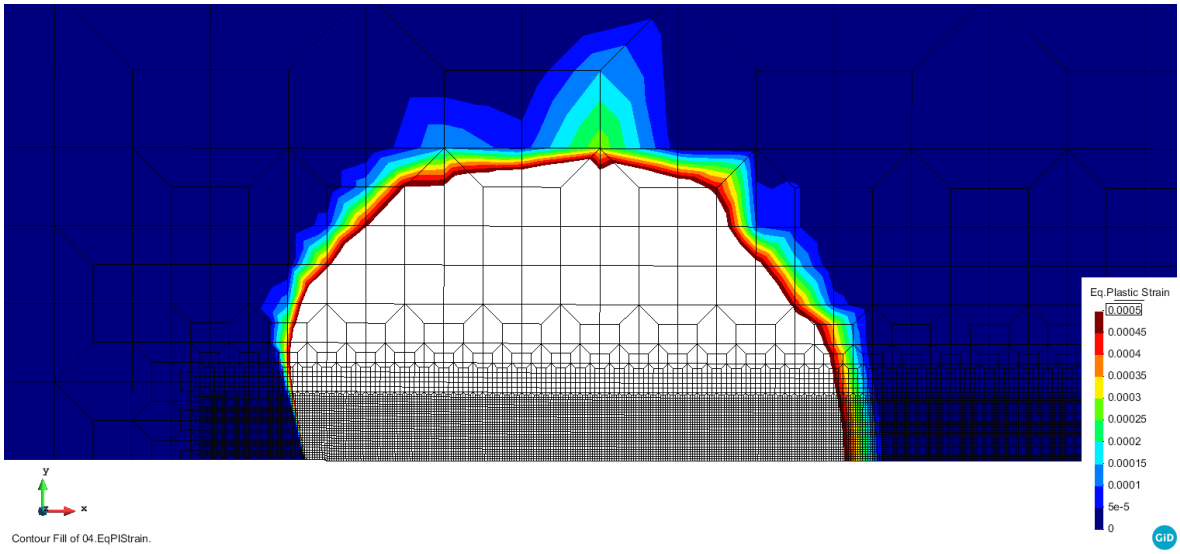


(b)

**Figure 4.19 – Plastically deformed zone for $a = 15.30$ mm: (a) Christmas Tree (15-9) pattern; (b) Christmas Tree (9-3) pattern.**

Figure 4.20 shows the plastically deformed zone from simulations of non-contact variable amplitude loading. The size of the plastically deformed zone is identical to the one obtained in the simulations with contact (see Figure 4.19).

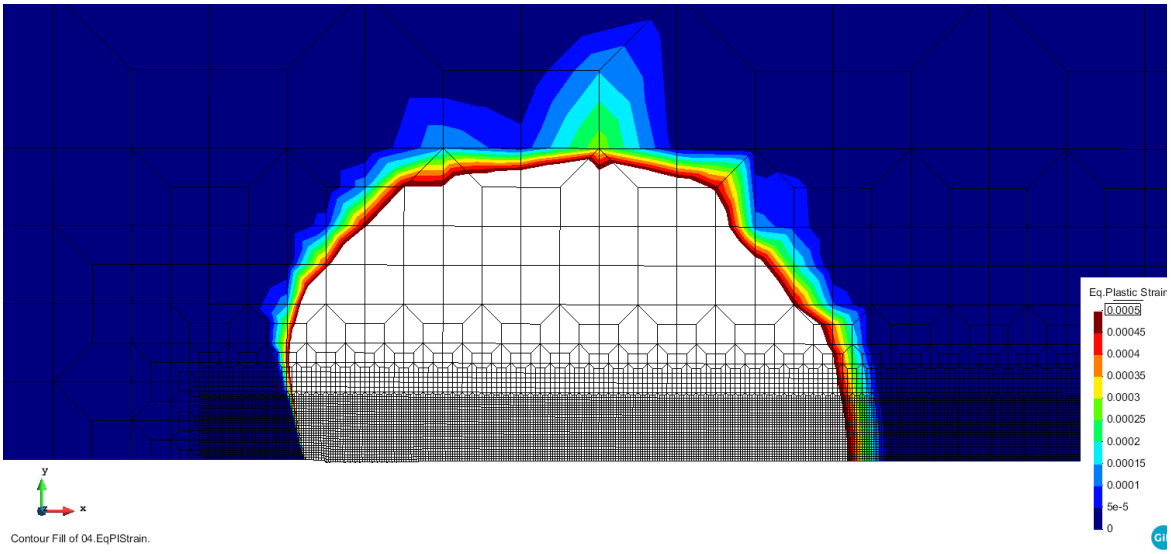


(a)

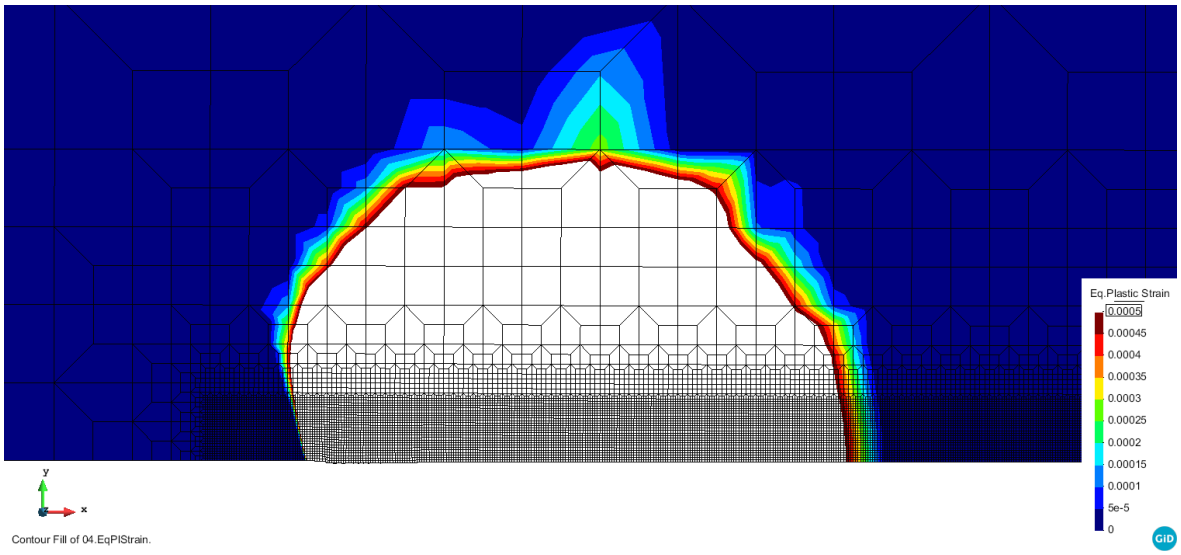


(b)

**Figure 4.20 – Plastically deformed zone for $a = 15.30$ mm in non-contact simulations: (a) Christmas Tree (15-9) pattern; (b) Christmas Tree (9-3) pattern.**

## 4.5. Stress Distribution

### 4.5.1. Constant Amplitude Loading

Figure 4.21 presents the distribution of the vertical component of the stress evaluated at the instant of minimum load, considering constant amplitude load patterns. The level of stress distribution in High Frequency pattern is less noticeable than in the Low Frequency because the maximum load is lower. Note that at the crack tip, the stresses are negative (compressive) due to plastic deformation near the crack. Considering the Low Frequency

pattern, the transition between compressive and tensile stresses occurs 24 μm after the crack tip. Note that, the stress distribution of the Low Frequency pattern is similar to the one obtained in the Christmas Tree patterns (see Figure 4.23) due to the load range.

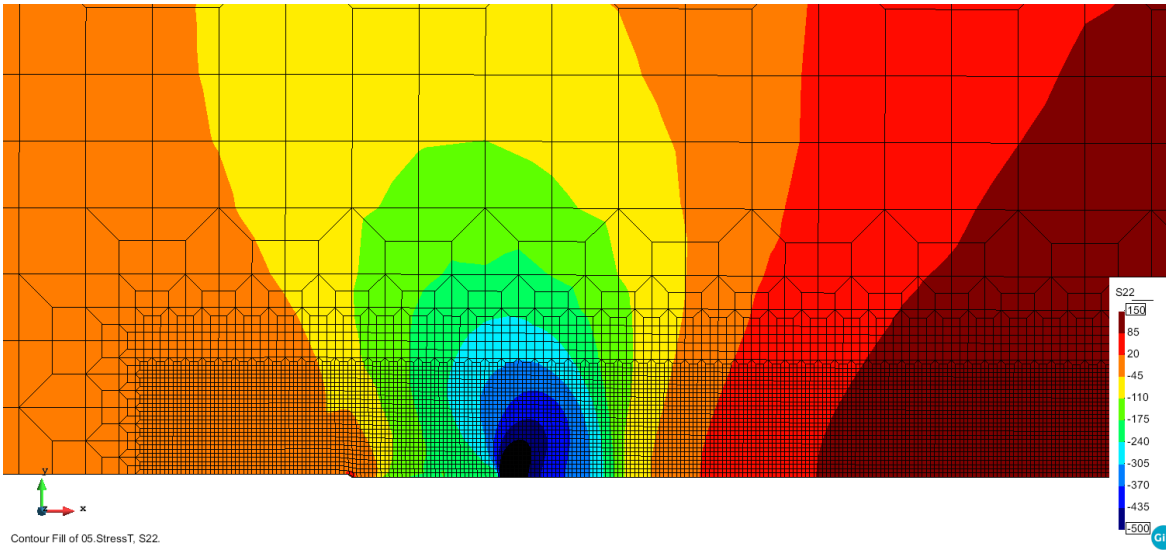


(a)

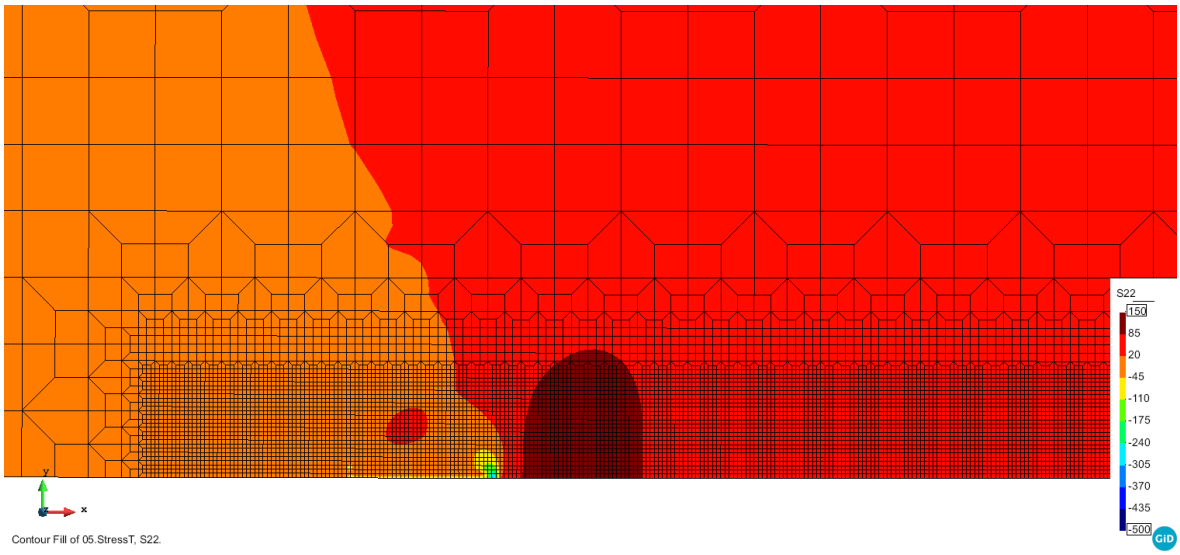


(b)

**Figure 4.21 – Stress distribution for $a = 15.30$ mm: (a) Low Frequency pattern; (b) High Frequency pattern.**

The distribution of the vertical component of the stress evaluated at the instant of minimum load, for non-contact simulation is presented in Figure 4.22. The stress distribution behind the crack tip is almost zero in the absence of contact (see Figure 4.22), while in simulations with contact the values are compressive. (see Figure 4.21). There are no compressive stresses before the crack, i.e., at the crack flanks, because there is no crack

closure in the non-contact simulations, so there is no resistance to the movement of the crack flank and therefore no compressive stresses are generated.

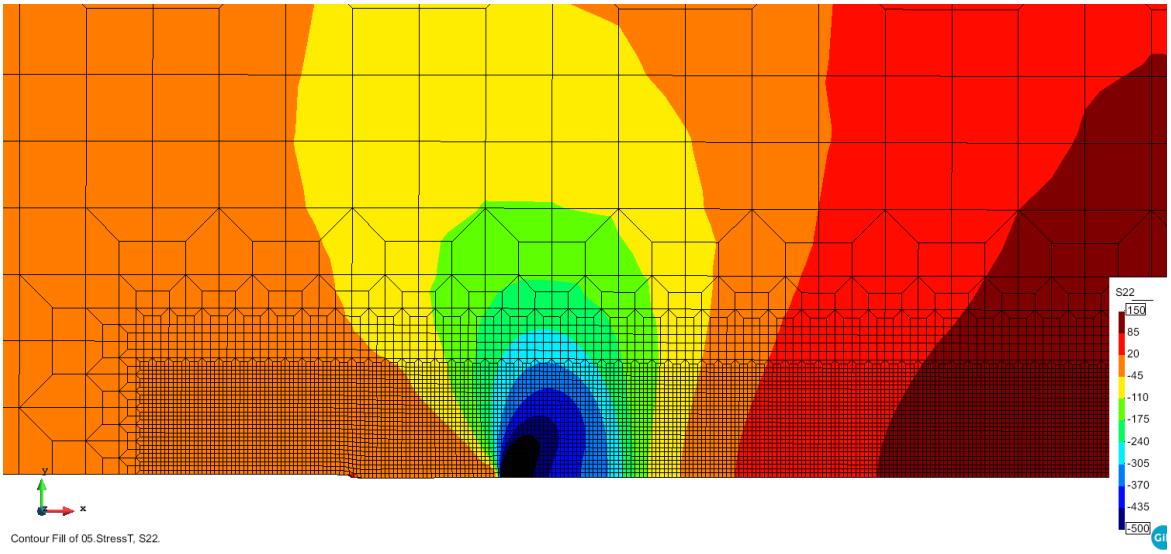


(a)

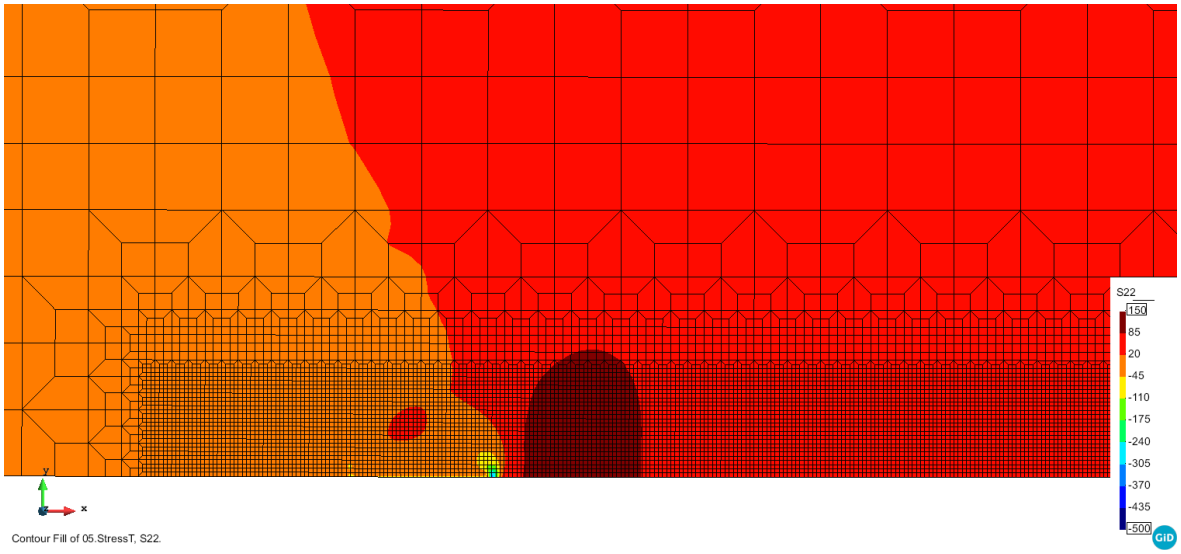


(b)

**Figure 4.22 – Stress distribution for $a = 15.30$ mm in non-contact simulations: (a) Low Frequency pattern; (b) High Frequency pattern.**

## 4.5.2. Variable Amplitude Loading

Figure 4.23 shows the vertical stress component field predicted for each variable amplitude loading pattern, evaluated near the crack tip at the instant of minimum load. The stress distributions of the variable amplitude loadings are very similar. The transition between compressive and tensile stresses occurs at 368 μm ahead of the crack tip for a crack length, $a = 15.30$ mm. Despite the loading history and kinematic strain hardening, the stress

distribution of the Low Frequency pattern (see Figure 4.21) is identical to the one obtained in the Christmas Tree patterns due to the similar load range.

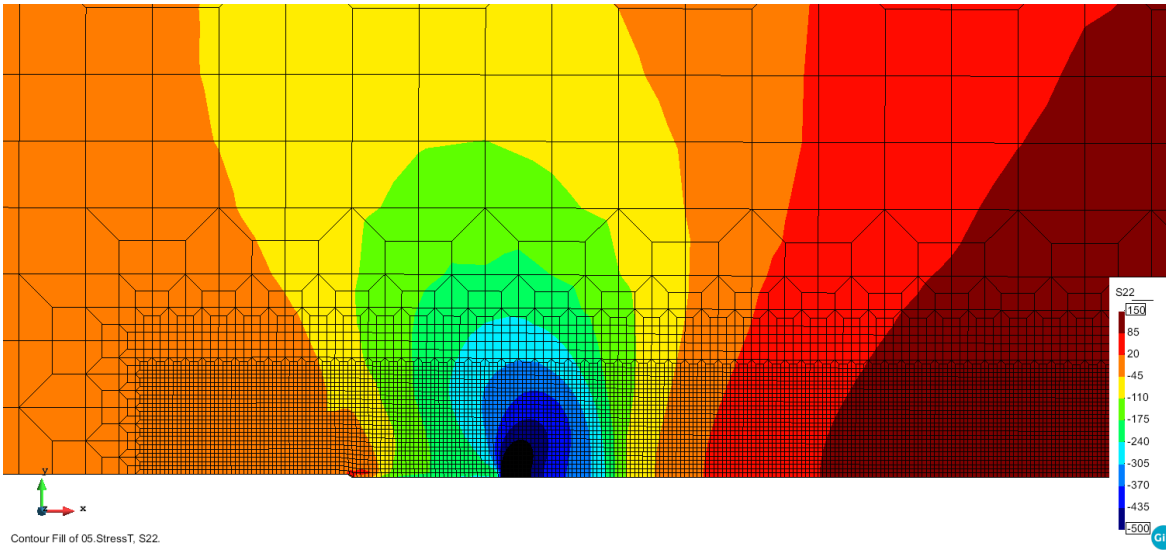


(a)

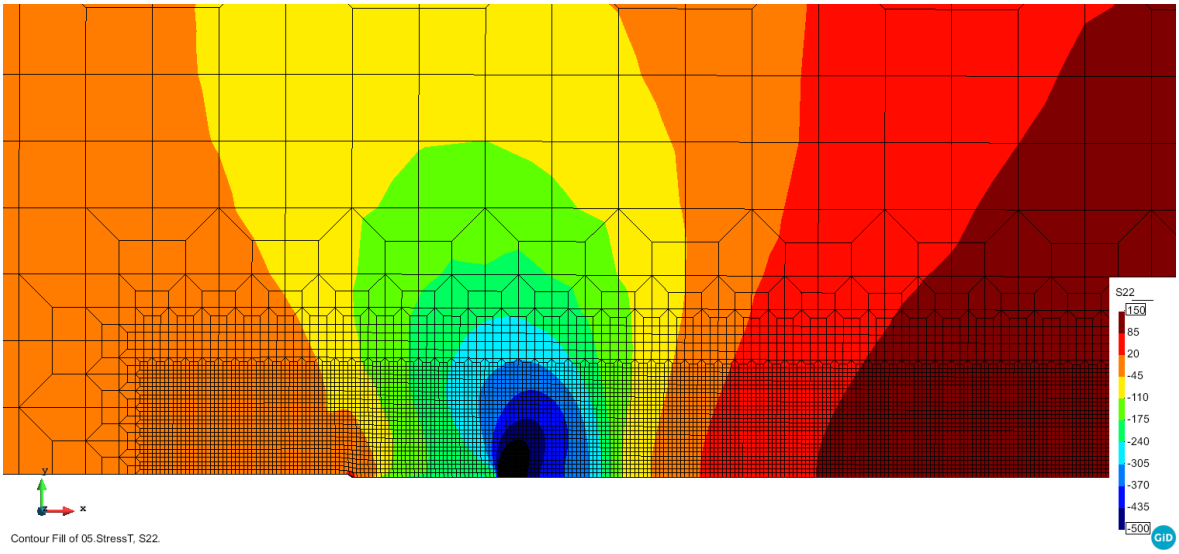


(b)

**Figure 4.23 – Stress distribution for $a = 15.30$ mm: (a) Christmas Tree (15-9) pattern; (b) Christmas Tree (9-3) pattern.**

Figure 4.24 shows the stress distribution from simulations of non-contact variable amplitude loading. In these stress distributions the same phenomenon that happened for the constant amplitude loading patterns, occurs. This is the crack closure phenomenon influences the stress distribution before the crack. Unlike the High Frequency loading pattern, this phenomenon is very noticeable for both the Low Frequency pattern and variable amplitude loading patterns.

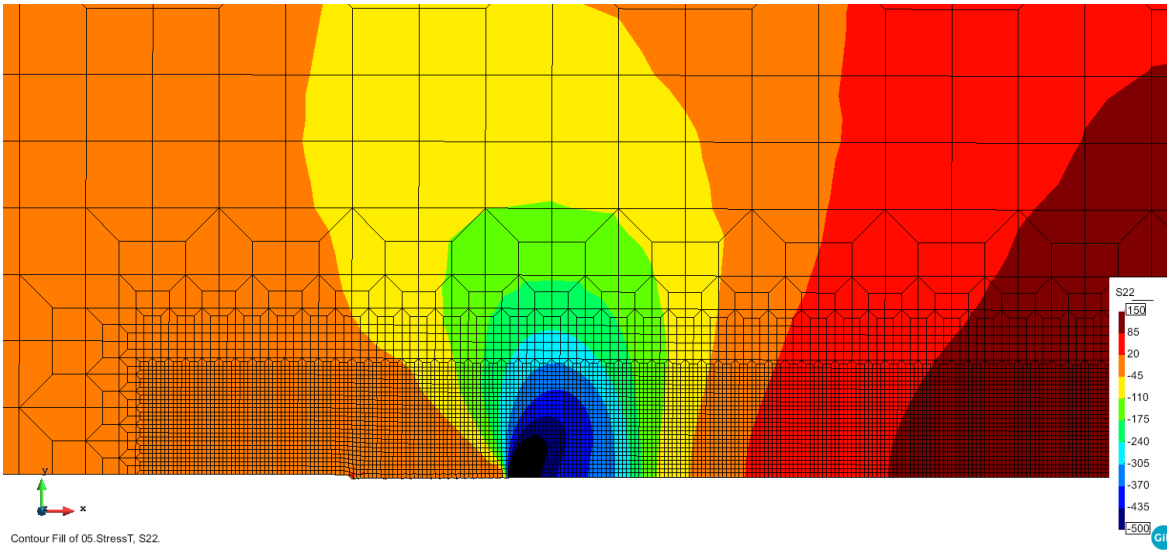


(a)

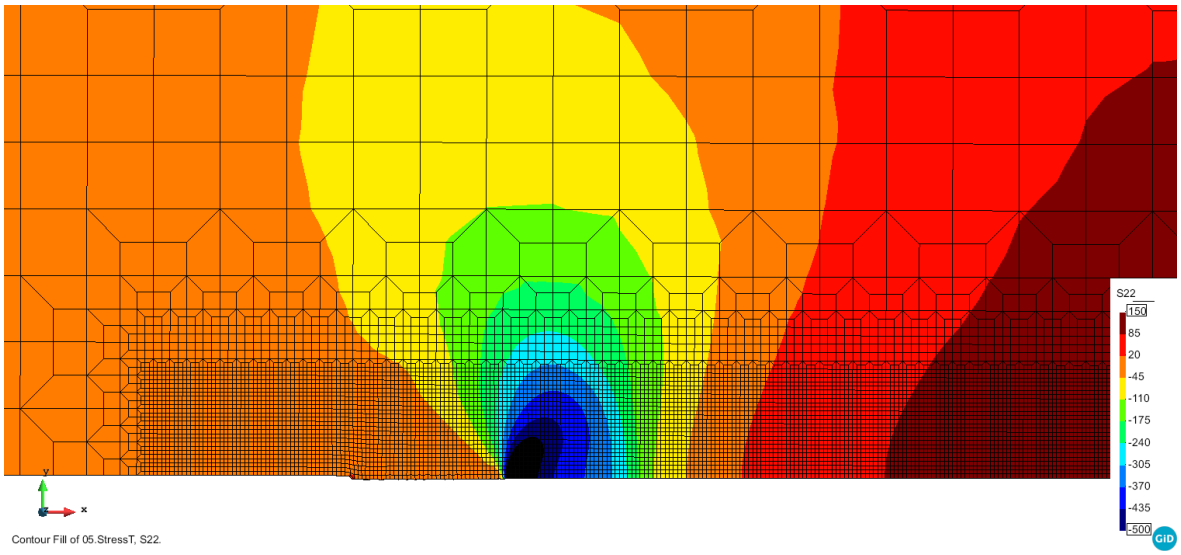


(b)

**Figure 4.24 – Stress distribution for $a = 15.30$ mm in non-contact simulations: (a) Christmas Tree (15-9) pattern; (b) Christmas Tree (9-3) pattern.**

# 5. CONCLUSIONS

In this thesis a numerical study on the effect of variable amplitude loadings on FCG was carried out. The so-called Christmas Tree loading pattern is compared with constant amplitude loading patterns. The numerical model used the cumulative plastic deformation at the crack tip as fatigue crack growth driving force. Through the obtained numerical results, it is possible to draw some more important conclusions:

- Considering the same value of minimum and maximum load, the crack propagation rates of the variable amplitude and constant amplitude loading patterns are similar. On the other hand, the inexistence of contact between the crack flanks increases $da/dt$ since the plastic strain growth rate is larger due to the absence of crack closure.
- The CTOD curves are similar for the various simulations except for the High Frequency pattern due to its loading amplitude. For the variable amplitude loads, without crack flanks contact, the CTOD curves undergo translations because crack propagation occurs at any time during the cycle. Despite this phenomenon, for patterns whose loading amplitude is equal, the shapes of the CTOD curves are quite similar.
- Despite the differences in the loading pattern, the plastic deformation tends to the same limit value, considering equal time intervals. The same occurs for the non-contact simulations, but here plastic strain tends to a higher maximum value. In general, the plastic deformation rise, is essentially evident at the end of each loading phase, when the maximum value of the applied force is reached. On the other hand, when the unloading phase is being applied, the plastic deformation is more evident at the end of the cycle, when the value of the applied force is lower.
- The size of the plastic zone for both Christmas Tree patterns, and the Low Frequency pattern is identical. Besides, there is no significant influence of the contact between crack fanks on in the size of the deformed zone.
- The stress gradient of the High Frequency pattern is much smaller compared to the other simulations. On the other hand, the stress gradients of the other

simulations are extremely similar for both the contact and non-contact simulations. The non-contact simulations do not exhibit compressive stresses behind the crack tip since closure phenomenon does not exist.

Following on from this dissertation, it would be important to further study the effect of variable amplitude loads, evolving to load patterns that replicate real loads. In this sense, there is the possibility of generating normalized load patterns, namely:

- TWIST – Transport WIng Standard, representative of the lower skin wing root of transport aircraft;
- FALSTAFF – Fighter Aircraft Loading STAndard For Fatigue evaluation;
- Helix – Standardised loading sequence for a helicopter main rotor (hinged);
- Felix – Standardised loading sequence for a helicopter main rotor (fixed);
- WISPER – Standardised loading sequence for wind turbines.

In this context it will be important to identify the fundamental mechanisms responsible for fatigue crack propagation and to study the material effect. The comparison of numerical predictions with experimental results obtained for the same loading patterns will be important for the validation of the numerical models.

# REFERENCES


[1] C. Moura Branco, J. Martins Ferreira, J. Domingos da Costa, and A. Silva Ribeiro, *Projecto de Orgãos de Máquinas*. 2012.

[2] Q. Xin, "Diesel engine system design," in *Woodhead Publishing*, 2011.

[3] K. Samadian, S. Hertelé, and W. De Waele, "Measurement of CTOD along a surface crack by means of digital image correlation," *Eng. Fract. Mech.*, vol. 205, pp. 470–485, Jan. 2019, doi: 10.1016/J.ENGFRACMECH.2018.11.015.

[4] M. F. Borges, D. M. Neto, and F. V Antunes, "Revisiting Classical Issues of Fatigue Crack Growth Using a Non-Linear Approach," *Materials (Basel).*, 2020, doi: 10.3390/ma13235544.

[5] F. V. Antunes, S. M. Rodrigues, R. Branco, and D. Camas, "A numerical analysis of CTOD in constant amplitude fatigue crack growth," *Theor. Appl. Fract. Mech.*, vol. 85, pp. 45–55, Oct. 2016, doi: 10.1016/J.TAFMEC.2016.08.015.

[6] L. F. Menezes and C. Teodosiu, "Three-dimensional numerical simulation of the deep-drawing process using solid finite elements," *J. Mater. Process. Technol.*, vol. 97, no. 1–3, pp. 100–106, Jan. 2000, doi: 10.1016/S0924-0136(99)00345-3.

[7] M. C. Oliveira, J. L. Alves, and L. F. Menezes, "Algorithms and Strategies for Treatment of Large Deformation Frictional Contact in the Numerical Simulation of Deep Drawing Process," *Arch. Comput. Methods Eng. 2008 152*, vol. 15, no. 2, pp. 113–162, Feb. 2008, doi: 10.1007/S11831-008-9018-X.

[8] A. Humanes Cisnal, "Technological and conceptual leaps on bridges: leading sector of technological experimentation during the last two centuries," Dec. 15, 2015. https://oa.upm.es/43676/ (accessed Jul. 02, 2022).

[9] Y. L. Lee and M. Guo, "Pseudo Stress Analysis Techniques," *Met. Fatigue Anal. Handb.*, pp. 61–87, Jan. 2012, doi: 10.1016/B978-0-12-385204-5.00002-1.

[10] P. Paris and F. Erdogan, "A Critical Analysis of Crack Propagation Laws," *J. Basic Eng.*, vol. 85, no. 4, p. 528, 1963.

[11] F. Erdogan and M. Ratwani, "Fatigue and fracture of cylindrical shells containing a circunferential crack," *Int. J. Fract. Mech*, vol. 6, no. 4, pp. 379–392, 1970.

[12] A. Hartman and J. Schijve, "The effects of environment and load frequency on the

crack propagation law for macro fatigue crack growth in aluminium alloys," *Eng. Fract. Mech.*, vol. 1, no. 4, pp. 615–631, Apr. 1970, doi: 10.1016/0013-7944(70)90003-2.

[13] G. R. Irwin, "Elasticity and Plasticity," in *Elasticity and Plasticity*, 6th ed., vol. 3, Berlin, 1958, pp. 551–590.

[14] J. R. Rice, "Mechanics of Crack Tip Deformation and Extension by Fatigue," *Fatigue Crack Propag.*, p. 247, Jan. 1967.

[15] A. Trudel, "Recent trends in the design of hydropower components subjected to cycling and fatigue; towards improved technical design specifications," *Hydrovision Int. 2017*, 2017, Accessed: Jun. 04, 2022. [Online]. Available: https://www.researchgate.net/publication/320310804_Recent_trends_in_the_design_of_hydropower_components_subjected_to_cycling_and_fatigue_towards_improved_technical_design_specifications

[16] T. L. Anderson, "Fracture Mechanics : Fundamentals and Applications," Mar. 2017, doi: 10.1201/9781315370293.

[17] B. Marques, M. F. Borges, F. V. Antunes, J. M. Vasco-Olmo, F. A. Díaz, and M. N. James, "Limitations of small-scale yielding for fatigue crack growth," *Eng. Fract. Mech.*, vol. 252, p. 107806, Jul. 2021, doi: 10.1016/J.ENGFRACMECH.2021.107806.

[18] W. Elber, "Fatigue Crack Closure Under Cyclic Tension," *Eng. Fract. Mech.*, vol. 2, pp. 37–45, 1970.

[19] L. M. Pedroso de Moura Correia, "Previsão da Vida de Propagação à Fadiga," PhD Thesis, Department of Mechanical Engineering, University of Coimbra, 2018.

[20] R. O. Ritchie, S. Suresh, and C. M. Moss, "Near-Threshold Fatigue Crack Growth in 2-1/4 Cr-1Mo Pressure Vessel Steel in Air and Hydrogen," *J. Eng. Mater. Technol.*, vol. 102, no. 3, p. 293, 1980.

[21] S. Suresh and R. O. Ritchie, "On the influence of fatigue underloads on cyclic crack growth at low stress intensities," *Mater. Sci. Eng.*, vol. 51, no. 1, pp. 61–69, 1981.

[22] S. Suresh and R. O. Ritchie, "A geometric model for fatigue crack closure induced by fracture surface roughness," *Met. Trans. A*, vol. 13, no. 9, pp. 1627–1631, 1982.

[23] F. V. Antunes, "Fatigue crack growth in metallic materials," Provas de agregação, 2021.

[24] J. A. F. O. Correia *et al.*, "Modified CCS fatigue crack growth model for the AA2019-T851 based on plasticity-induced crack-closure," *Theor. Appl. Fract. Mech.*, vol. 85, pp. 26–36, Oct. 2016, doi: 10.1016/J.TAFMEC.2016.08.024.

[25] K. Donald and P. C. Paris, "An evaluation of ΔKeff estimation procedures on 6061-T6 and 2024-T3 aluminum alloys," *Int. J. Fatigue*, vol. 21, no. SUPPL. 1, pp. S47–S57, Sep. 1999, doi: 10.1016/S0142-1123(99)00055-9.

[26] D. Kujawski, "Enhanced model of partial crack closure for correlation of R-ratio effects in aluminum alloys," *Int. J. Fatigue*, vol. 23, no. 2, pp. 95–102, Jan. 2001, doi: 10.1016/S0142-1123(00)00085-2.

[27] M. Lugo and S. R. Daniewicz, "The influence of T-stress on plasticity induced crack closure under plane strain conditions," *Int. J. Fatigue*, vol. 33, no. 2, pp. 176–185, Feb. 2011, doi: 10.1016/J.IJFATIGUE.2010.08.002.

[28] S. G. Larsson and A. J. Carlsson, "Influence of non-singular stress terms and specimen geometry on small-scale yielding at crack tips in elastic-plastic materials," *J. Mech. Phys. Solids*, vol. 21, no. 4, pp. 263–277, Jul. 1973, doi: 10.1016/0022-5096(73)90024-0.

[29] C. J. Christopher, M. N. James, E. A. Patterson, and K. F. Tee, "Towards a new model of crack tip stress fields," *Int. J. Fract.*, vol. 148, pp. 361–371, 2007, doi: 10.1007/s10704-008-9209-3.

[30] R. Hosseini and | R Seifi, "Influence of Hardening on the Cyclic Plastic Zone Around Crack Tip in Pure Copper CT Specimens," *J. Stress Anal.*, vol. 2, no. 2, 2018, doi: 10.1111/ffe.12862.

[31] A. A. Wells, "Unstable Crack Propagation in metals, Cleavage and Fast Fracture," *Crack Propag. Symp. Cranf.*, vol. 1, no. 84, pp. 210–230, 1961.

[32] J. R. Rice, "A Path Independent Integral and the Approximate Analysis of Strain Concentration by Notches and Cracks," *J. Appl. Mech.*, vol. 35, no. 2, pp. 379–386, Jun. 1968, doi: 10.1115/1.3601206.

[33] X. K. Zhu, P. Zelenak, and T. McGaughy, "Comparative study of CTOD-resistance curve test methods for SENT specimens," *Eng. Fract. Mech.*, vol. 172, pp. 17–38, Mar. 2017, doi: 10.1016/J.ENGFRACMECH.2017.01.007.

[34] B. Marques, L. P. Borrego, J. M. Ferreira, F. V. Antunes, and R. Branco, "A numerical analysis of fatigue crack closure using CTOD," *Procedia Struct. Integr.*, vol. 18, pp.

645–650, Jan. 2019, doi: 10.1016/J.PROSTR.2019.08.211.

[35] F. V Antunes, R. Branco, P. A. Prates, and L. Borrego, "Fatigue crack growth modelling based on CTOD for the 7050-T6 alloy," *Fatigue Fract Engng Mater Struct*, vol. 40, pp. 1309–1320, 2017, doi: 10.1111/ffe.12582.

[36] M. Skorupa, "Load Interaction Effects During Fatigue Crack Growth Under Variable Amplitude Loading—A Literature Review. Part I: Empirical Trends," *Fatigue Fract. Eng. Mater. Struct.*, vol. 21, no. 8, pp. 987–1006, Aug. 1998, doi: 10.1046/J.1460-2695.1998.00083.X.

[37] O. E. Wheeler, "Spectrum Loading and Crack Growth," *J. Basic Eng.*, vol. 94, no. 1, pp. 181–186, Mar. 1972, doi: 10.1115/1.3425362.

[38] S. Mikheevskiy and G. Glinka, "Elastic–plastic fatigue crack growth analysis under variable amplitude loading spectra," *Int. J. Fatigue*, vol. 31, no. 11–12, pp. 1828–1836, Nov. 2009, doi: 10.1016/J.IJFATIGUE.2009.02.035.

[39] A. H. Noroozi, G. Glinka, and S. Lambert, "A two parameter driving force for fatigue crack growth analysis," *Int. J. Fatigue*, vol. 27, pp. 1277–1296, 2005, doi: 10.1016/j.ijfatigue.2005.07.002.

[40] M. Skorupa, "Load interaction effects during fatigue crack growth under variable amplitude loading—a literature review. Part II: qualitative interpretation," *Fatigue Fract. Eng. Mater. Struct.*, vol. 22, no. 10, pp. 905–926, Oct. 1999, doi: 10.1046/J.1460-2695.1999.00158.X.

[41] A. H. Noroozi, G. Glinka, and S. Lambert, "A study of the stress ratio effects on fatigue crack growth using the unified two-parameter fatigue crack growth driving force," *Int. J. Fatigue*, vol. 29, pp. 1616–1633, 2007, doi: 10.1016/j.ijfatigue.2006.12.008.

[42] X. Huang, M. Torgeir, and W. Cui, "An engineering model of fatigue crack growth under variable amplitude loading," *Int. J. Fatigue*, vol. 30, no. 1, pp. 2–10, Jan. 2008, doi: 10.1016/J.IJFATIGUE.2007.03.004.

[43] W. Elber, "The significance of fatigue crack closure. Damage tolerance in aircraft structures," *ASTM STP 486*, pp. 230–242, 1971.

[44] J. Silva, "Efeito de carregamentos de amplitude variável na propagação de fendas por fadiga," University of Coimbra, 2021.

[45] T. Endo, K. Mitsunaga, K. Takahashi, K. Kobayashi, and M. Matsuishi, "Fatigue of

metals subjected to varying stress," *Japan Soc. Mech. Eng.*, 1974.

[46] T. Endo, K. Mitsunaga, K. Takahashi, K. Kobayashi, and M. Matsuishi, "Damage evaluation of metals for random or varying loading. Proceedings of the 1974 Symposium on Mechanical Behavior of Materials," *Soc. Mater. Sci.*, vol. 1, pp. 371–380, 1974.

[47] Yung-Li Lee, Mark E. Barkey, and Hong-Tae Kang, *Metal Fatigue Analysis Handbook: Practical problem-solving techniques for computer-aided engineering*, vol. 3. 2011.

[48] F. D. Richards, N. R. LaPointe, and R. M. Wetzel, "A Cycle Counting Algorithm for Fatigue Damage Analysis on JSTOR." https://www.jstor.org/stable/44734430?seq=1 (accessed Jun. 04, 2022).

[49] S. D. Downing and D. F. Socie, "Simple rainflow counting algorithms," *Int. J. Fatigue*, vol. 4, no. 1, pp. 31–40, Jan. 1982, doi: 10.1016/0142-1123(82)90018-4.

[50] C. Amzallag, J. P. Gerey, J. L. Robert, and J. Bahuaud, "Standardization of the rainflow counting method for fatigue analysis," *Int. J. Fatigue*, vol. 16, no. 4, pp. 287–293, Jun. 1994, doi: 10.1016/0142-1123(94)90343-3.

[51] Jagabandhu Chakrabarty, *Applied Plasticity*, Second Edition. 2010.

[52] R. Hill, *The Mathematical Theory of Plasticity*. UK: Oxford, 1950.

[53] P. Prates, "Inverse Methodologies for Identifying Constitutive Parameters of Metal Sheets," PhD Thesis, Department of Mechanical Engineering, University of Coimbra, 2014.

[54] H. W. Swift, "Plastic instability under plane stress," *J. Mech. Phys. Solids*, vol. 1, no. 1, pp. 1–18, Oct. 1952, doi: 10.1016/0022-5096(52)90002-1.

[55] J. Lemaitre and J.-L. Chaboche, *Mechanics of Solid Materials*, 1st ed. Press Sindicate of the University of Cambridge, 1994.

[56] M. F. Borges *et al.*, "Fatigue crack propagation analysis in 2024-T351 aluminium alloy using nonlinear parameters," *Int. J. Fatigue*, vol. 153, p. 106478, Dec. 2021, doi: 10.1016/J.IJFATIGUE.2021.106478.

[57] F. V. Antunes, D. Camas, L. Correia, and R. Branco, "Finite element meshes for optimal modelling of plasticity induced crack closure," *Eng. Fract. Mech.*, vol. 142, pp. 184–200, Jul. 2015, doi: 10.1016/J.ENGFRACMECH.2015.06.007.

[58] E. Rafael and A. Sérgio, "ANÁLISE DA PROPAGAÇÃO DE FENDAS POR

FADIGA UTILIZANDO O MODELO DE DANO GTN,” 2021.

# APPENDIX A

This section presents the comparison charts for each simulation with contact.

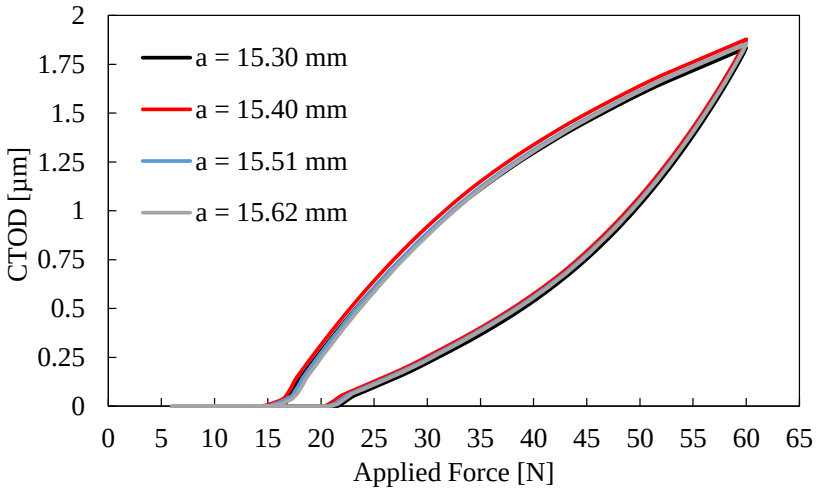


**Figure A.1 – Effect of crack length on CTOD curves for the Low Frequency simulation with contact.**

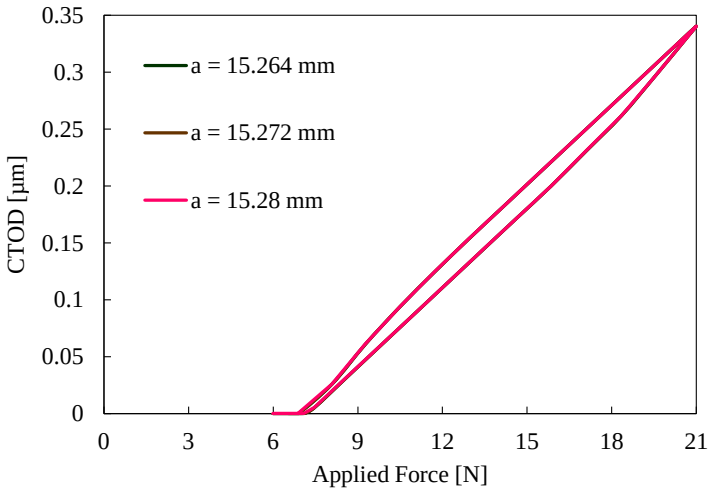


**Figure A.2 – Effect of crack length on CTOD curves for the High Frequency simulation with contact.**

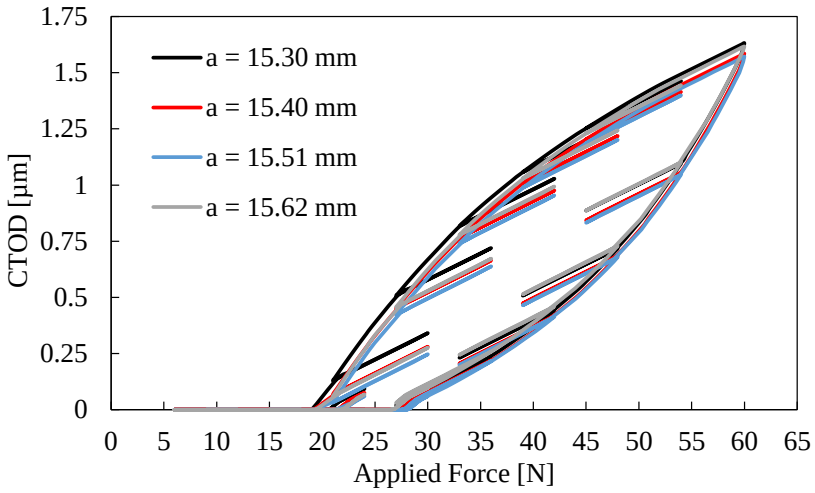


**Figure A.3 – Effect of crack length on CTOD curves for the Christmas Tree (15-9) simulation with contact.**

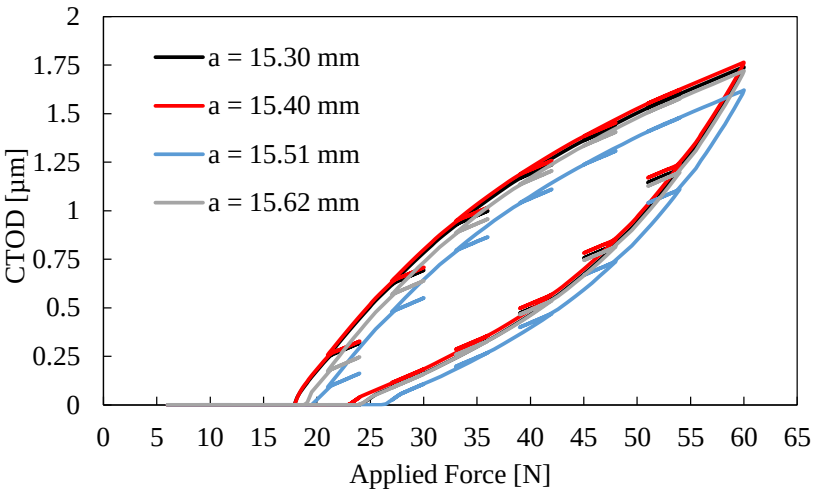


**Figure A.4 – Effect of crack length on CTOD curves for the Christmas Tree (9-3) simulation with contact.**

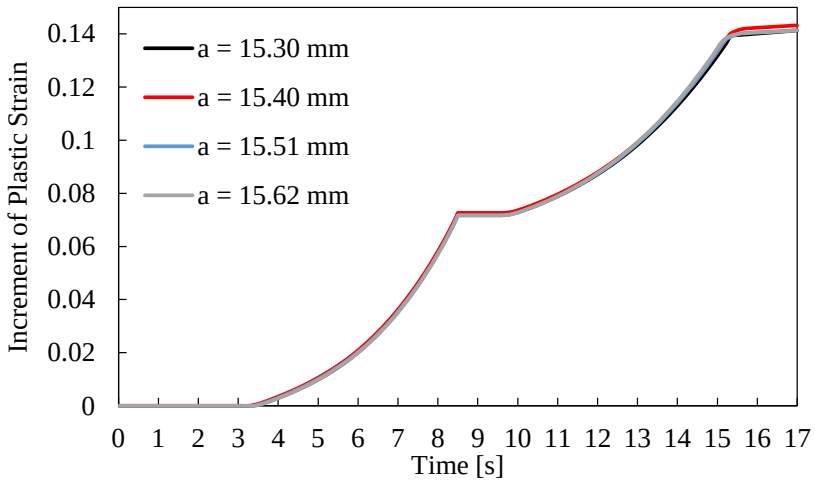


**Figure A.5 – Effect of crack length on plastic strain curves for the Low Frequency simulation with contact.**

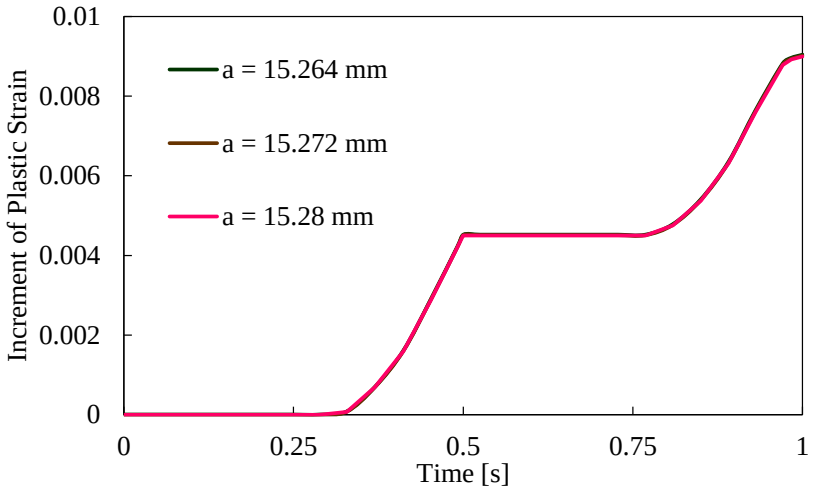


**Figure A.6 – Effect of crack length on plastic strain curves for the High Frequency simulation with contact.**

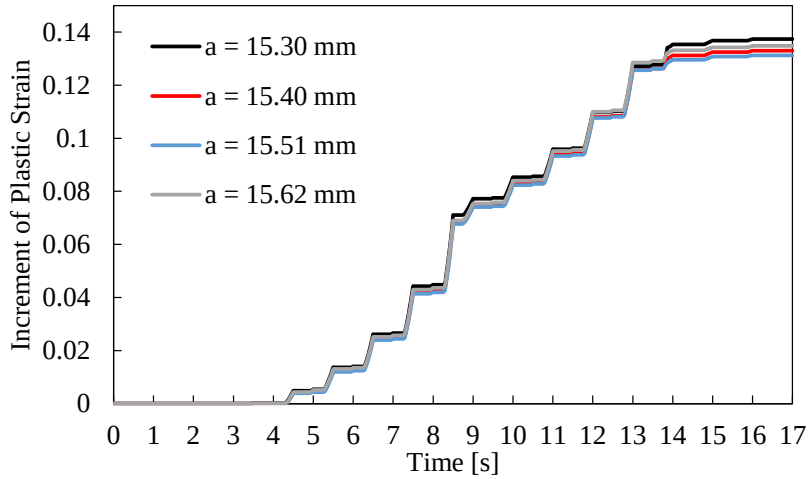


**Figure A.7 – Effect of crack length on plastic strain curves for the Christmas Tree (15-9) simulation with contact.**

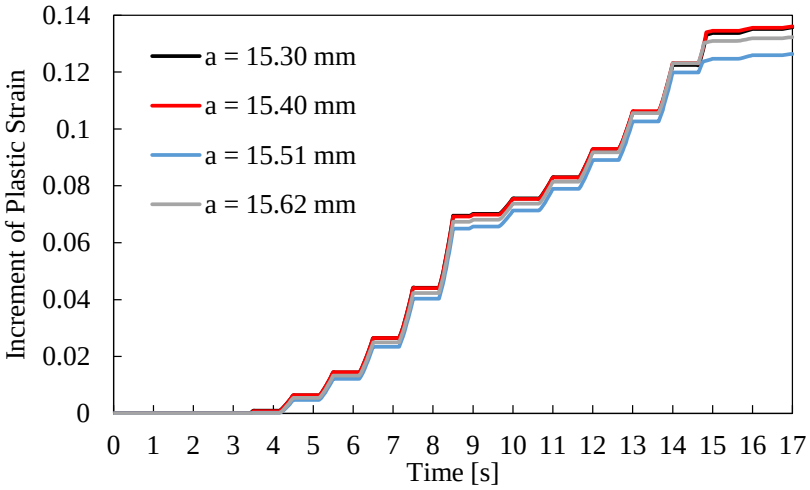


**Figure A.8 – Effect of crack length on plastic strain curves for the Christmas Tree (9-3) simulation with contact.**

# APPENDIX B

This section presents the comparison charts for each contactless simulation.

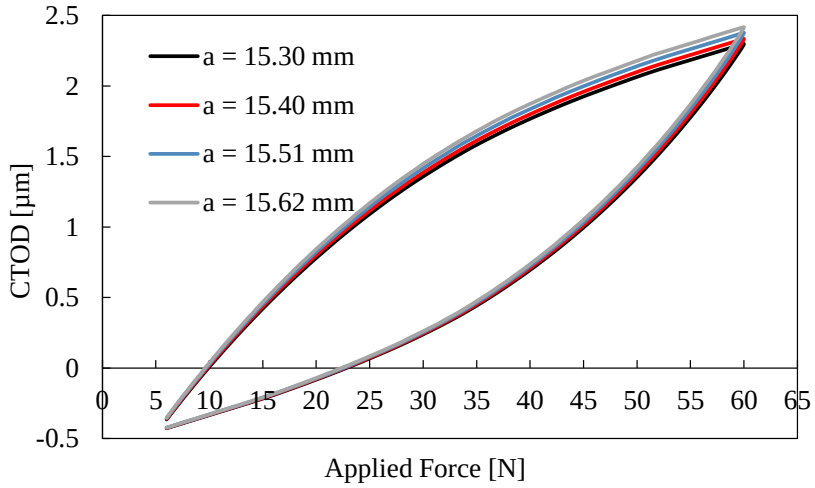


**Figure B.1 – Effect of crack length on CTOD curves for the Low Frequency simulation without contact.**

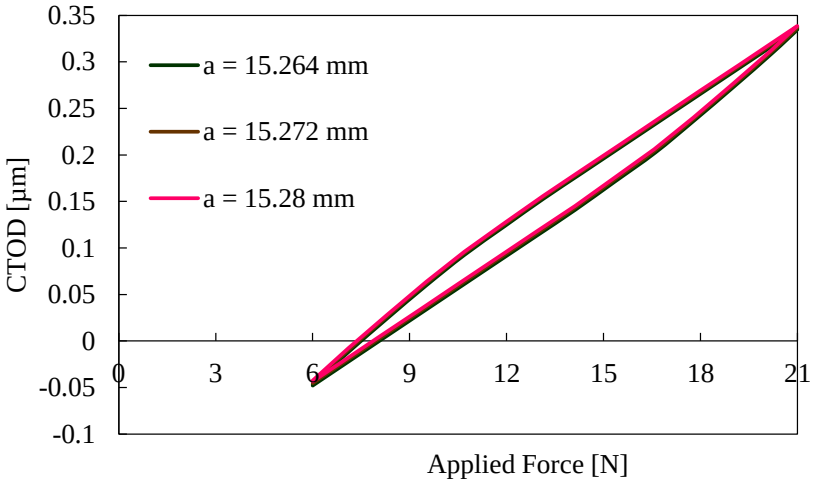


**Figure B.2 – Effect of crack length on CTOD curves for the High Frequency simulation without contact.**

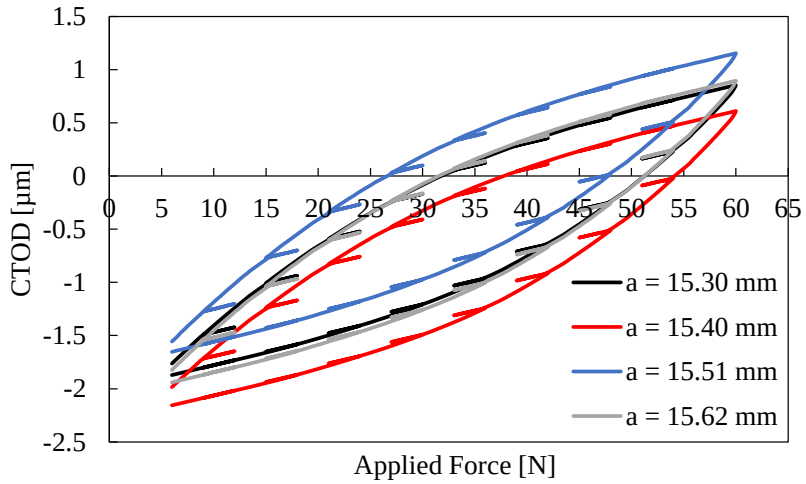


**Figure B.3 – Effect of crack length on CTOD curves for the Christmas Tree (9-3) simulation without contact.**

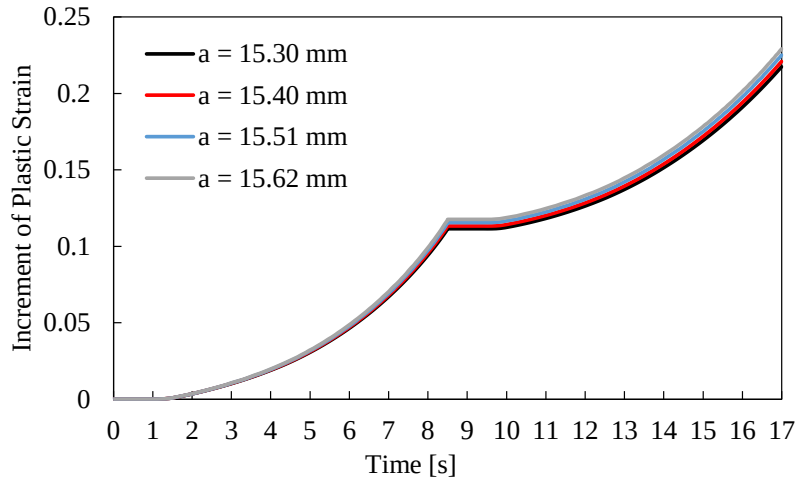


**Figure B.4 – Effect of crack length on plastic strain curves for the Low Frequency simulation without contact.**

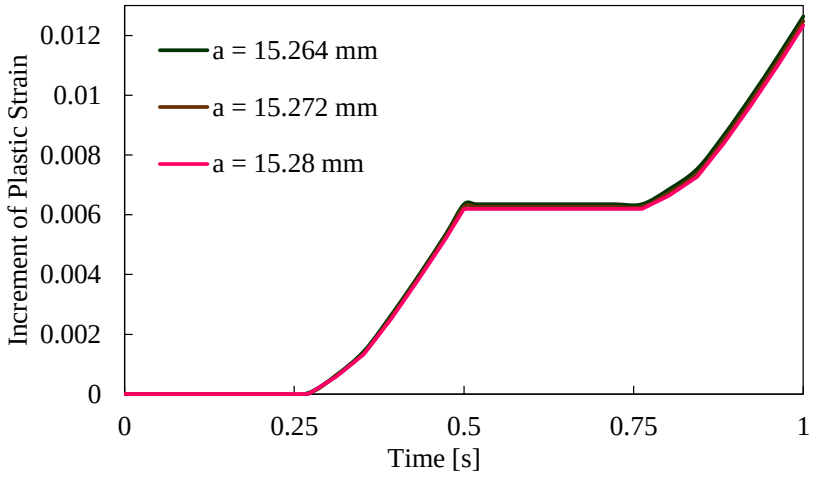


**Figure B.5 – Effect of crack length on plastic strain curves for the High Frequency simulation without contact.**

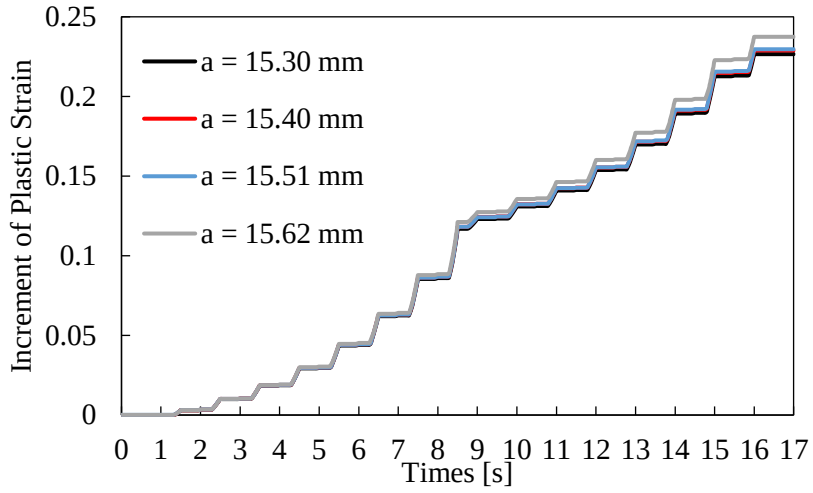


**Figure B.6 – Effect of crack length on plastic strain curves for the Christmas Tree (15-9) simulation without contact.**

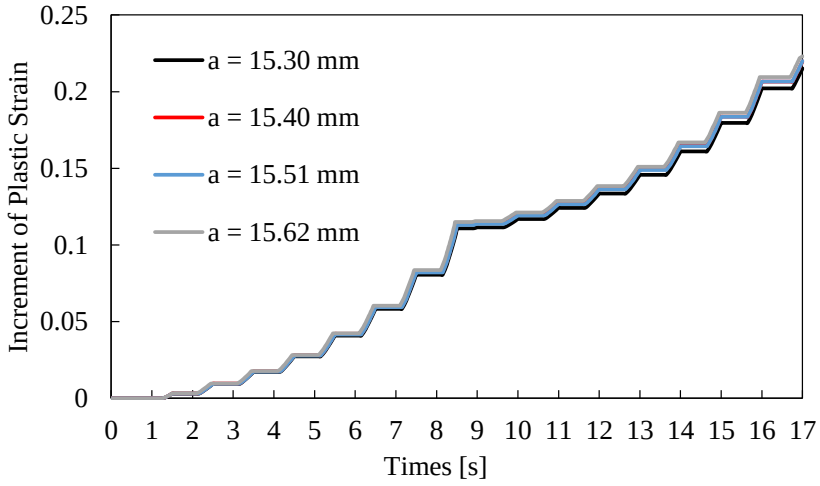


**Figure B.7 – Effect of crack length on plastic strain curves for the Christmas Tree (9-3) simulation without contact.**